Journal of Inflammation Research

Dovepress
Taylor & Francis Group

Open Access Full Text Article

ORIGINAL RESEARCH

Interleukin-1 Receptor-Associated Kinase-3 Aggravates Neuroinflammatory Injury After Intracerebral Hemorrhage via Activation NF-κB/IL-17A Pathway in Mice

Jun Wang[1]*, Yulong Li[1]*, Chunyu Tan[1]*, Jinlian Shao[1], Weitai Tang[2], Quan Kong[3], Wenqianjun Sheng[1], Zhiquan Ding[1], Feng Li[1], Jifeng Piao[1], Dingyi Lv[1], Libin Hu[1], Qinghua Wang[1], Xiaodan Jiang[1]

[1]Neuromedicine Center, The National Key Clinical Specialty, The Engineering Technology Research Center of Education Ministry of China on Diagnosis and Treatment of Cerebrovascular Disease, Guangdong Provincial Key Laboratory on Brain Function Repair and Regeneration, The Neurosurgery Institute of Guangdong Province, Guangdong-Hong Kong-Macao Greater Bay Area Center for Brain Science and Brain-Inspired Intelligence, Zhujiang Hospital, Southern Medical University, Guangzhou, 510282, People's Republic of China; [2]Department of Neurosurgery, The People's Hospital of Luoding & Affiliated Luoding Hospital of Guangdong Medical University, Luoding, 527200, People's Republic of China; [3]Neurosurgery Department of Zengcheng Campus, Nanfang Hospital, Southern Medical University, Guangzhou, People's Republic of China

*These authors contributed equally to this work

Correspondence: Qinghua Wang; Xiaodan Jiang, Email wqh1123@126.com; jiangxiao_dan@163.com

Background: Neuroinflammatory reactions are crucial factors in secondary brain damage following intracerebral hemorrhage (ICH). Although previous studies have shown that IRAK3 is involved in immune responses, the potential effects of IRAK3 on ICH remain unclear.

Methods: Collagenase IV–induced ICH mouse model. Western blotting was used to determine the expression of IRAK3 at different time points following ICH. Immunofluorescence was used to investigate the cellular localization of IRAK3. The ICH model was treated with recombinant human IRAK3 (rh-IRAK3) or IRAK3 siRNA via an intracerebroventricular injection. The effect of IRAK3 on ICH mice was assessed by Western blotting and short-term and long-term neurological function evaluation. RNA-seq was performed to explore the mechanism by which IRAK3 promotes inflammation after ICH. The mechanisms of IRAK3 and neuroinflammation will be further investigated by Western blotting, qRT-PCR and immunofluorescence. Recombinant IL-17A was used to investigate the connection between IRAK3 and the NF-κB/IL-17A signaling pathway in vivo and in vitro experiments.

Results: The expression of IRAK3 increased, peaking at 24 h, followed by a subsequent decrease after ICH. IRAK3 is mainly expressed in the microglia. RNA-seq analysis revealed 1,797 differentially expressed genes around the perihematomal brain tissue after IRAK3 siRNA treatment, with multiple inflammatory pathways being downregulated. Rh-IRAK3 treatment resulted in upregulation of the levels of inflammatory cytokines around the perihematomal tissue and exacerbated neurological function deficits. Furthermore, IRAK3 siRNA treatment markedly decreased the expression of inflammatory cytokines and microglial activation via the NF-κB/IL-17A signaling pathway. Recombinant IL-17A exacerbated the inflammatory response in vivo and in vitro; however, IRAK3 knockdown reversed this process.

Conclusion: IRAK3 aggravates neuroinflammation by activating the NF-κB/IL-17A signaling pathway, thereby exacerbating neurological deficits following ICH. Therefore, inhibition IRAK3 may be a promising approach for treating ICH.

Keywords: IRAK3, neuroinflammation, intracerebral hemorrhage, microglia, NF-κB/IL-17A pathway

Introduction

Intracerebral hemorrhage (ICH), a prevalent form of stroke, has a 1-year survival rate of less than 50%. Survivors commonly experience neurological and cognitive disabilities.[1] Brain injuries following ICH can be divided into primary and secondary brain injuries (SBI). Primary brain injury is caused by the space-occupying effect of the hematoma, which

Received: 19 September 2024
Accepted: 8 January 2025
Published: 25 January 2025

directly compresses and damages brain tissue. Secondary brain injury begins and progresses in the hours following ICH, leading to a cascade of adverse consequences over the subsequent days to weeks. The mechanisms underlying SBI include excitotoxicity, mediated by glutamate release, thrombin activation, neuroinflammation, blood-brain barrier disruption, apoptosis, and necrosis.[2] Poor outcomes associated with ICH are predominantly attributable to SBI.[3]

Neuroinflammation following ICH is a crucial factor contributing to neurological deficits in patients.[4] The by-products of blood trigger a cytotoxic response in brain parenchymal cells, including an inflammatory reaction, blood-brain barrier disruption, neuronal apoptosis, and cellular death by necrosis.[5,6] Previous studies have shown that microglia are among the first responders to blood-derived breakdown materials with an inflammatory process.[7] Activated microglia release an abundance of pro-inflammatory mediators including chemokines, reactive oxygen species, and cytokines, thereby aggravating the inflammatory response.[8,9] The NF-κB targets include cytokines, chemokines, and various inflammatory protein enzymes.[10] Moreover, excessive inflammation leads to increased blood-brain barrier permeability, thereby precipitating cerebral edema. Cerebral edema intensifies ischemia and hypoxia in the tissues surrounding the hematoma, amplifying the inflammatory reaction.[11] Therefore, attenuation of neuroinflammatory response may be an effective therapeutic approach for treating ICH.

Interleukin-1 receptor-associated kinase 3 (IRAK3) is a member of the IRAK family, initially described as an NF-κB-induced inflammatory signaling mediator.[12,13] While IRAK3 activation has been shown to confer neuroprotection in cerebral ischemia and Alzheimer's disease, it paradoxically promotes neuroinflammation in the EAE model.[14–17] Additionally, IRAK3 has been implicated in regulating epithelial cell inflammation.[18,19] Obviously, the role of IRAK3 in modulating inflammation across different diseases was different. However, its role in neuroinflammation after ICH is unknown. Moreover, the lack of specific IRAK3 inhibitors has hindered the development of therapeutic strategies for ICH. Therefore, this study aims to investigate the role of IRAK3 in a mouse model of ICH and explore its underlying mechanisms, providing a theoretical basis for the development of therapeutic targets for ICH. Specifically, we focus on the activation of the IL-17A signaling pathway and its potential roles with IRAK3, as it is a crucial pathway involved in promoting inflammation and neuronal toxicity following ICH.[20]

Here, we hypothesize that inhibiting IRAK3 may downregulate the NF-κB/IL-17A signaling pathway, thereby reducing neuroinflammation and promoting neurological recovery after ICH. Consequently, targeting IRAK3 might be a promising approach for ICH treatment.

Methods

Animals and ICH Animal Model

C57BL/6 male mice aged 10–12 weeks and weighing 25–30 g, were selected for this study. All specific pathogen-free (SPF) mice were acquired from the Experimental Animal Center of Southern Medical University and housed with appropriate temperature and humidity, and a 12-hour light/dark cycle, and free access to food and water. All experimental designs, surgical procedures, and animal care and management procedures were approved by the Ethics Committee of the Zhujiang Hospital of Southern Medical University (Animal Ethics No. LAEC-2023-156) and complied with the guidelines of the National Institute of Health.

As previously described,[21] anesthesia was induced in mice by intraperitoneal injection of 1.25% tribromoethanol (0.2 mL/10 g). Once the mice were in a deep anesthetic state, they were fixed on a brain stereotaxic apparatus. The hair on the head was shaved and the scalp was fully exposed. After disinfecting the scalp with iodophor, the skin was held with the thumb and forefinger and a midline incision was made to expose the bregma and lambda. The puncture site was marked 2 mm laterally from the center of the anterior fontanelle, and then 0.2 mm in the anterior direction. The drill bit was removed upon experiencing a breakthrough. A sterile 5 μL microsyringe was then used to aspirate 1.0 μL of collagenase, and the needle was carefully guided in a straight, vertical direction into the burr hole until it reached 3.5 mm a depth. After 5 min, collagenase was administered to the right striatum at a flow rate of 0.25 μL/min. To prevent backflow of collagenase, the needle was left in its original position for an additional 5 min. Upon needle removal, the burr hole was promptly sealed with bone wax, followed by disinfection and suturing of the incision site. Finally, the mice were returned to their cages to ensure that they remained warm.

Experiment Design and Group

The sample sizes for each group were determined based on those used in previous similar studies.[21–24]

Experiment 1: To investigate the time-dependent dynamic changes in IRAK3 expression and cellular localization following ICH. Mice were allocated to sham, ICH 3h, ICH 6h, ICH 12h, ICH 24h, and ICH 48h groups, with 3 mice in each group (n=3). WB was used to detect the expression of IRAK3 at different time points after ICH. Mice were allocated to sham and ICH groups to detect the expression level of IRAK3 by immunohistochemistry and immunofluorescence experiments, with 3 mice in each group (n=3). The injury condition around hematoma was observed by HE after ICH (Figure 1A).

Experiment 2: To explore the effect of IRAK3 expression levels on SBI following ICH, mice were divided into five groups: sham, ICH+Vehicle, ICH+rh-IRAK3 1μg group, ICH+rh-IRAK3 3μg group, and ICH+rh-IRAK3 5μg group, with 6 mice in each group (n=6). The optimal therapeutic dose was selected based on the behavioral assessment scores. Mice were allocated into sham, ICH+Vehicle, and ICH+rh-IRAK3 groups. 3 mice for each group (n=3). The expression of inflammatory factors in the different groups was detected using Western blotting after ICH 24h. Using the optimal dosage of rh-IRAK3 to treat mice with ICH, the mice were divided into three groups: sham, ICH+Vehicle, and ICH + rh-IRAK3, 6 mice in each group (n=6). Neurofunctional deficits in the mice were assessed using a neurological scoring tests 72 hours after ICH (Figure 1B).

Experiment 3: To investigate the effect of endogenous IRAK3 knockdown on neuroinflammation after SBI following ICH, mice were allocated to the ICH+Vehicle group and ICH+IRAK3 siRNA group, 5 mice in each group (n=5). RNA

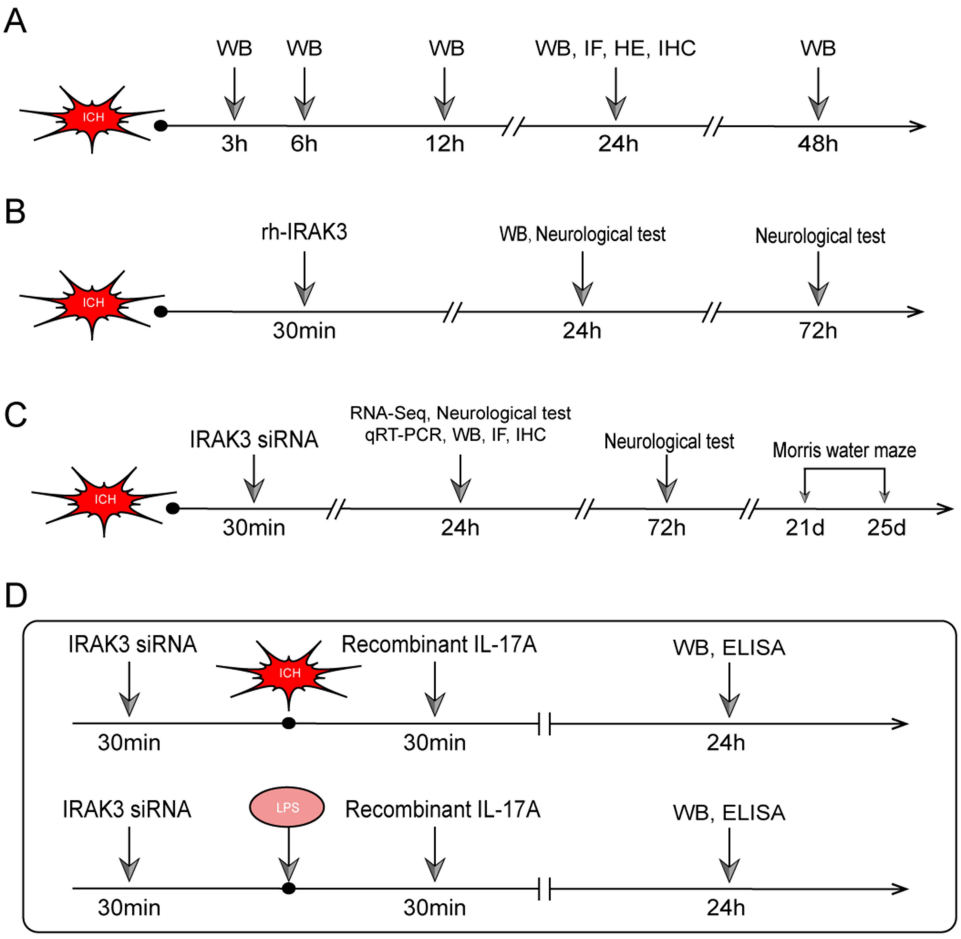

Figure 1 Experimental design layout. (**A**) Patterns of IRAK3 expression and its anatomical distribution after ICH. (**B**) The impact of IRAK3 on neuroinflammatory processes and neurological function deficits after ICH. (**C**) Evaluating the influence of IRAK3 knockdown on neuroinflammatory processes and both short-term and long-term neurological function deficits after ICH. (**D**) Exploring the relationship between IRAK3 and the NF-κB/IL-17A signaling pathway in vivo and vitro.

https://doi.org/10.2147/JIR.S494611

sequencing (RNA-Seq) was performed. Mice were allocated into sham, ICH+Vehicle, and ICH+IRAK3 siRNA groups, with 6 mice in each group (n=6), undergoing neurological function tests at 24 h and 72 h after ICH. Additionally, the Morris water maze test was conducted on 21–25 days to evaluate cognitive function, n=6. Mice that completed the neurological function assessment at 24h were subjected to qRT-PCR, WB, IF, and IHC experiments, n=3 (Figure 1C).

Experiment 4: To investigate the mechanism by which IRAK3 regulates neuroinflammation, we conducted in vivo and in vitro experiments using recombinant IL-17A and IRAK3 siRNA. In the in vivo experiments, mice were randomly divided into five groups: sham group, ICH +Vehicle group, ICH+IRAK3 siRNA group, ICH+IL-17A+Vehicle group, and ICH+IL-17A+IRAK3 siRNA group, each with 3 mice (n=3). Thirty minutes before ICH was established, IRAK3 siRNA was injected into the lateral ventricles. Following the successful establishment of the ICH model for 30 min, recombinant IL-17A was injected into the contralateral ventricle. The tissue surrounding the hematoma was harvested for WB and enzyme-linked immunosorbent assay (ELISA) to detect the expression levels of NF-κB, IL-17A, IL-1β, IL-18, IL-6 and TNF-α after ICH for 24h. BV2 microglial cells were cultured in vitro and stimulated with lipopolysaccharide (LPS) to simulate the inflammatory environment following ICH. The cells were divided into five groups: control, LPS + Vehicle, LPS + IRAK3 siRNA, LPS + IL-17A + Vehicle, and LPS + IL-17A + IRAK3 siRNA. After the addition of recombinant IL-17A and IRAK3 siRNA, we conducted WB and ELISA experiments after 24h to evaluate the expression levels of NF-κB, IL-17A, IL-1β, IL-18, IL-6 and TNF-α, n=3 (Figure 1D).

Blinding and Inclusion/Exclusion Criteria

All mice were assigned sequential numbers generated randomly by a computer program, and the allocations were masked from the investigators to prevent bias. The exclusion criteria comprised mice exhibiting ICH with no or minimal hematoma, as well as those that experienced intraoperative or preoperative mortality. During the neurological function assessments, the investigators were blinded to the group assignments and the treatments administered.

Sample Preparation

The pre-prepared brain tissue was removed and allowed to reach room temperature. An appropriate amount of peri-hematoma brain tissue was weighed, thoroughly ground, and placed in a 2 mL EP tube. RIPA lysis buffer, protease inhibitor, and phosphatase inhibitor were added at a ratio of 100:1:1 and the tissue was lysed on ice for 30 min. If the tissue grinding was ineffective, a sonicator was used for further disruption. Three grinding steel beads were added to the lysis solution. The grinding parameters were set as 70 hz/90 s/-20°C. After grinding, the lysate was stored on ice for an additional 20 minutes of digestion. The EP tube containing the lysate was then placed in a refrigerated high-speed centrifuge and centrifuged at 4°C for 15 minutes at 14000 rpm. The protein solution was transferred to a new 1.5 mL EP tube, taking care not to disturb the cell debris at the bottom. A small aliquot of the protein solution was used to determine protein concentration. The loading buffer working solution was added and the mixture was subsequently boiled for 15 min. The prepared protein samples were stored at −80°C for future use.

Drug Administration and Intracerebroventricular Injection

In vivo transfection was performed as previously described,[25,26] and IRAK3 siRNA (Obio Technology, Beijing, China) was transfected using an siRNA transfection reagent (Engreen Biosystems, Beijing, China). According to the protocol, IRAK3 siRNA was dissolved in RNase-free water at concentrations of 1, 2, and 3 μg/μL. An equivalent concentration of scrambled siRNA was transfected into the negative control group. The optimal concentration of IRAK3 siRNA was chosen based on the qRT-PCR results. rh-IRAK3 (Fine Biotech, Wuhan, China) was dissolved in sterile PBS to a final concentration of 1, 3, or 5 μg/μL. Recombinant IL-17A was purchased from eBioscience (San Diego, CA, USA). Based on a previous described,[27] the dose for intraventricular injection in in vivo experiments was 20 ng, whereas the concentration for in vitro experiments was 100 ng/mL. Mice were anesthetized with 1.25% tribromoethanol (0.2 mL/10 g). After shaving the hair on the head of the mice, the scalp was disinfected with 75% alcohol. The scalp was incised to fully expose the fontanelle. With the anterior fontanelle as the center, a cranial burr hole was drilled at a coordinate 0.2 mm posterior and 1.0 mm lateral to the fontanelle. Subsequently, rh-IRAK3 or IRAK3 siRNA was injected into the left ventricle of the mouse at a depth of 2.25 mm below the dura mater, and a release of 0.5 μL/min rate. The needle was

left in place for 5 min following injection, followed by slow withdrawal over 3 min. Finally, sterile medical bone wax was used to seal the cranial burr hole after the needle removal.

Cell Culture

IRAK3 is expressed not only in microglia but also in neurons and astrocytes. Given that microglia are the primary cells that induce neuroinflammation, we decided to focus our investigation on IRAK3's effects specifically in microglia. To minimize confounding factors, we conducted our studies in vitro using cultured microglial cells. BV2 microglial cells were obtained from Procell Life Science & Technology (Wuhan, China) and cultured in Dulbecco's modified Eagle's medium (DMEM) supplemented with 100 U/mL penicillin, 100 μg/mL streptomycin (Solarbio, Beijing, China), and 10% fetal bovine serum containing glucose. Cells were incubated at 37°C in a 5% CO2 atmosphere, seeded at a density of approximately 5×10^5 cells per well in a 6-well plate, and stimulated with 1 μg/mL LPS to simulate the inflammatory environment following ICH.

Cell Viability Assay

As previously described,[28] cell viability was assessed using the CCK-8 assay (Fdbio Science, China). Briefly, BV2 microglial cells were seeded at a density of 1×10^4 cells per well in 96-well plates and treated with varying concentrations of rh-IRAK3 or IRAK3 siRNA for 24 hours. Subsequently, 10 μL of CCK-8 solution was added to each well. After incubating at 37°C for 2 hours, absorbance at 450 nm was measured using a microplate reader (SYNERGY H1, BioTek, USA). Cell viability was determined based on the optical density (OD) values.

Western Blotting

As previously described,[28] brain tissue from the left basal region was rapidly collected after perfusion of the left atrium with 0.9% saline. Proteins were extracted from the left basal ganglia tissue with RIPA lysis buffer (Beyotime, China). The lysate was sonicated and thoroughly ground in a cryogenic grinder (Luca, China), centrifuged at 14,000 rpm for 15 min at 4°C, and the supernatant was collected. A BCA assay kit (Beyotime, China) was used to determine the protein concentration. The supernatant was mixed with a protein loading buffer (ComWin Biotech, China) and boiled for 15 min. Protein separation was achieved using gel electrophoresis and transferred onto a PVDF membrane (Millipore Sigma, USA). The PVDF membrane was blocked in 5% non-fat milk for 2 h, followed by overnight (15–18 hours) incubation with the diluted primary antibody at 4°C. Primary antibody information is presented in Table 1. After washing the membrane with TBST, it was incubated with the secondary antibody solution for 1.5 hours. Finally, enhanced chemiluminescent HRP substrate (Millipore Sigma, USA) was used to detect the target protein bands. β-actin was used as an internal control. ImageJ software was used to measure the band intensities.

Immunofluorescence Staining

As previously described,[29] after full-body anesthesia, the left ventricular apex was perfused with 100 mL of pre-cooled 4% paraformaldehyde. Upon completion of perfusion, the brain was immersed in 4% paraformaldehyde for 24 h, transferred to a 30% sucrose solution, and incubated at 4 °C until the suspended brain tissue sank to the bottom. The brain tissue was embedded using OCT embedding medium (Sakura, USA) and then sectioned into 10 μm coronal slices. The cryosections were washed with PBS, immersed in sodium citrate-EDTA antigen retrieval solution, and boiled for 10 min. The sections were incubated with a 10% goat serum solution for 2 h in a humid chamber. The solution was discarded and the primary antibody (Table 1) was added and incubated for 15–18h at 4°C. The unbound primary antibody was washed away with PBS and the sample was incubated for 2 h at room temperature with the secondary antibody. Nuclei were labeled with DAPI and the slides were subsequently coverslipped. Images were obtained using a Ti2E fluorescence microscope (Nikon, Japan). The ImageJ software was used to quantify the number of cells in the images.

RNA-Seq Analysis

The sequencing process involved a multistage procedure, sample preparation, and sample quality assessment. This is followed by library construction that requires rigorous quality control. High-throughput sequencing is then conducted,

Table 1 Table of Antibodies Used

Antibody Name	Host Spices and Clone	Manufacturer	Usage	Dilution Ratio	Identifier
IRAK3	Rabbit monoclonal	Novus	WB, IF, IHC	WB = 1:2000 IF = 1:200 IHC = 1:50	NBP1-76782
IBA-1	Mouse polyclonal	Servicebio	WB, IF	1:300	GB12105-100
GFAP	Mouse polyclonal	Abcam	IF	1:300	Ab279290
IL-1β	Rabbit polyclonal	Proteintech	WB	1:1500	26,048-1-AP
TNF-α	Rabbit polyclonal	Proteintech	WB	1:1000	17,590-1-AP
IL-18	Rabbit Polyclonal	Proteintech	WB	1:2000	10,663-1-AP
IL-6	Rabbit Polyclonal	Proteintech	WB	1:1000	29,444-1-AP
IL-17A	Rabbit polyclonal	Proteintech	WB, IF, IHC	WB= 1:1000 IF= 1:200 IHC= 1:100	26,163-1-AP
NF-κB/pNF-κB	Rabbit monoclonal	Abcam	WB	1:2000	Ab16502 ab76302
β-actin	Rabbit polyclonal	Beyotime	WB	1:1000	AF5003
Rabbit IgG (HPR)	Goat	Beyotime	WB	1:10000	A0208
Mouse IgG (HPR)	Goat	Beyotime	WB	1:10000	A0216
Goat Anti- Rabbit/Mouse IgG H&L (Alexa Fluor® 488)	Goat	Abcam	IF	1:1000	Ab150077 Ab150113
Goat Anti- Rabbit/Mouse IgG H&L (Alexa Fluor® 647)	Goat	Abcam	IF	1:1000	Ab150083 Ab150115

succeeded by data quality control protocols. Ultimately, the workflow concludes with a bioinformatics analysis. 24 hours after the successful establishment of the ICH model, peri-hematoma tissue samples were collected from both the ICH group and ICH + IRAK3 siRNA group. Total RNA was isolated using the TRIzol method, and its concentration and purity were determined using the RNA Nano 6000 Assay Kit. Double-stranded cDNA was generated by reverse transcription and qualified fragments were selected and amplified by PCR to obtain the sequencing library. After successful quality control, the library was sequenced on an Illumina NovaSeq 6000 platform (Biomarker Technologies, China). Because there were no outliers among the samples, further analyses were performed. Differential analysis was conducted using R software. The edgeR package is used to normalize FPKM values and identify significantly differentially expressed RNAs. Edgers were used for the differential expression analysis. Genes were considered differentially expressed if the fold change>1.5 and the p-value<0.05,[30] and a heatmap is generated using the R package based on the normalized values of all DEGs. A volcano plot is created to visualize the consistently significant DEGs between the two cohorts. Gene Ontology (GO) and Kyoto Encyclopedia of Genes and Genomes (KEGG) pathway analyses were conducted to annotate the potential functions of the differentially expressed genes (DEGs). A false discovery rate (FDR) of < 0.05 was set as the significance threshold for enriched GO terms and KEGG pathways. Additionally, as previously described, Gene Set Enrichment Analysis (GSEA) was performed using the clusterProfiler R package to analyze DEGs between the two cohorts. Gene sets were analyzed based on KEGG and Reactome pathways, with enriched gene sets assigned according to a nominal FDR < 0.05.[31,32] The data were deposited

in the CNGB Sequence Archive (CNSA) of the China National GeneBank DataBase (CNGBdb) under accession number SUB057791 (https://db.cngb.org/cnsa/).

Neurological Score Test

As previous study described,[28] the modified Garcia scoring system to evaluate neurological function in mice, which comprises seven distinct assessment items. These items are categorized based on their scoring ranges: four items, including spontaneous activity, symmetry of limb movement, body proprioception, and extending forelimbs, are scored on a scale of 0 to 3, while three items, namely climbing ability, sensory response, and lateral turning, are scored on a scale of 1 to 3. Specifically, spontaneous activity was assessed by observing the mouse's self-initiated movements in a new cage for 5 minutes, yielding scores from 0 (no activity) to 3 (active exploration). Body proprioception was evaluated by lifting the tail and noting the angle and range of lateral turning, resulting in scores from 0 (no turning) to 3 (smooth and coordinated turning). Similarly, sensory response was determined by gently stimulating the whiskers using a cotton swab, yielding scores from 1 (no response) to 3 (clear reaction). Furthermore, the extension of forelimbs was observed during tail lifting, resulting in scores from 0 (no extension) to 3 (full extension). Axial sensation was assessed by lightly touching both sides of the body with a stick, yielding scores between 1 (no response) and 3 (noticeable response). Additionally, symmetry of limb movement was evaluated by observing the movement of all four limbs when the tail was lifted, with scores ranging from 0 (no movement) to 3 (fully coordinated movement). Finally, climbing ability was assessed on an inclined surface, with scores ranging from 1 (unable to climb) to 3 (proficient climbing). The total score, which ranges from a minimum of 3 to a maximum of 21 points, represents a cumulative assessment of neurological function, where a lower score indicates more severe neurological deficits.

A corner turning test was conducted by setting up two partitions at a 30-degree angle to the table surface. The mouse was gently encouraged to walk towards the corners formed by the two partitions. When the mouse entered the corner, it instinctively chose to turn it. Each mouse was tested 10 times, with a 30-second interval between trials. Given the potential for damage to the right basal ganglia in the experimental model, the focus was on recording the frequency of left turns made by the mouse during 10 trials, which was then expressed as a percentage.

The forelimb placement test assesses the motor response of the mouse forelimbs to tactile stimulation. After ensuring that the mouse's limbs were in a relaxed, non-tensed state, the mouse was slowly brought to the edge of a table and one of its whiskers lightly touched the table surface. The researcher then observed whether the mouse forelimb extended naturally towards the table edge when the whisker contacted the surface. Each mouse was tested 10 times, with a 30-second interval between trials, and the frequency of successful forelimb extension towards the table edge was recorded. Given the potential damage to the right basal ganglia in the experimental model, only the frequency of left forelimb extension was calculated and expressed as a percentage.

The Morris water maze test was completed on days 21–25 after ICH to assess memory and spatial learning capacity. As previous study described,[33] a circular pool with a diameter of 120 cm was filled with an opaque white liquid and evenly divided into four quadrants. A platform with a diameter of 5 cm was positioned at the center of one quadrant. During the first 5 days of training, the platform was submerged approximately 1 cm below the water surface, and mice were placed into the pool from four different starting positions, with each trial lasting 60 seconds. On the 6th day, the platform was removed, and the mice were placed into the pool from a fixed starting position. A camera recorded the mice's movements, and software was used to analyze the time required to find the platform during training, the time spent in the target quadrant after platform removal, and the number of times the mice crossed the former platform location.

qRT-PCR

As previously described,[29] perihematomal tissue was collected 24 h after ICH induction and the AG RNAex Pro RNA reagent was used to extract total RNA. A SYBR Green Pro Taq HS reverse transcription kit was used to generate cDNA. A Bio-Rad sequencing detection system was used for qRT-PCR analysis. GAPDH was used as an internal control. The $2^{-\Delta\Delta Ct}$ method was used to analyze the relative expression levels of the target genes. The primer sequences are shown in Table 2.

Table 2 Primers Used for qRT-PCR

Gene	Primer Sequences, 5′-3′ Forward	Reverse
IRAK3	GGTGGCAGGAAACATCTGTGGTAC	TTCCGAGGACAGGGTGGTATCTTC
IL-1β	TTCAGGCAGGCAGTATCACTCATTG	TTCAGGCAGGCAGTATCACTCATTG
IL-18	TTCAGGCAGGCAGTATCACTCATTG	TTCAGGCAGGCAGTATCACTCATTG
TNF-α	ATCCGCGACGTGGAACTG	ACCGCCTGGAGTTCTGGAA
IL-6	TTCTTGGGACTGATGCTGGTG	CACAACTCTTTTCTCATTTCCACGA
GAPDH	AGGTCGGTGTGAACGGATTTG	TGTAGACCATGTAGTTGAGGTGA

Hematoxylin and Eosin Staining

As previously described,[34] the mice were deeply anesthetized and administrated pre-cooled 0.1 M PBS (pH 7.4). Perfusion was switched from PBS to 4% paraformaldehyde once the liver turned white. The brain tissue was immersed in 4% paraformaldehyde for 24 h at 4°C. After dehydration and paraffin embedding, continuous coronal sections of 4 μm thickness were obtained. Briefly, brain sections were deparaffinized, rehydrated, and stained with hematoxylin and eosin. The staining duration was adjusted based on the desired staining intensity. Images were captured using an optical microscope (Leica-DM2500, Leica, Wetzlar, Germany), and the observers were blinded to the experimental groups.

IHC Staining

As previously described,[35] after the prepared brain tissue sections were dewaxed, rehydrated, and subjected to antigen retrieval, they were incubated with 3% hydrogen peroxide for 15 minutes. The brain tissue sections were then covered with 5% goat serum and incubated for 30 min. The primary antibody working solution was added and incubated at 4°C for 12–15 hours. The antibodies used for immunohistochemical staining were the same as those used for IF staining of IRAK3 and IL-17A. Subsequently, sections were incubated with biotinylated goat anti-rabbit antibody for 15 min. The sections were then incubated with horseradish peroxidase-streptavidin reagent for 15 min. Finally, the sections were stained with 3.3′-diaminobenzidine and hematoxylin. The sections were observed and images were obtained using an optical microscope (3D HISTECH, Dynamax Biotech, Shanghai, China) by personnel blinded to the experimental grouping.

ELISA Analysis

As previously described,[29] ELISA kits for IL-1β and TNF-α were purchased from R&D Systems (Minneapolis, USA). Briefly, the mice were deeply anesthetized and perfused transcardially with PBS, and brain tissues were quickly harvested. The samples were homogenized using a Dounce homogenizer (Thermo Fisher Scientific, USA) in buffer containing a protease inhibitor cocktail (Nacalai Tesque, Japan).

Statistical Analysis

Statistical analyses were performed using the GraphPad Prism software (version 10.1.2). Data are presented as the mean ± standard error of the mean (SEM). For comparison between more than two groups, one-way analysis of variance (ANOVA) was used. Post-hoc tests, including Bonferroni correction, were conducted for multiple comparisons. For non-normally distributed values, non-parametric ANOVA (Kruskal–Wallis test) was used, followed by Dunn's post-hoc test for multiple comparisons. Mann–Whitney *U*-tests were used for individual comparisons between independent values within groups. Additionally, two-way repeated measures ANOVA was used for the long-term Morris water maze test data. $P<0.05$ was considered statistically significant.

Results

The ICH Model and Mortality Rate

The overall mortality rate of experimental mice was 4.5% (7/155). In this study, no deaths occurred in the sham group. Mortality rates did not differ significantly among the treatment groups. Twenty mice were excluded due to the absence of hematomas in mice with ICH. No drug-related adverse reactions were observed in any of the treatment groups.

The Expression Pattern and Location of IRAK3 in Experimental Mouse ICH Model

Western blotting was used to investigate the expression of IRAK3 at 3, 6, 12, 24, and 48 h after the establishment of the ICH model. IRAK3 expression was markedly increased at 3 h, peaking at 24 h, and decreased at 48 h after ICH compared to sham group (Figure 2A amd B). Immunohistochemical analysis revealed that the expression of IRAK3 increased in the ICH group than in the sham group at 24 h (Figure 2D and E). Immunofluorescence staining co-labeled IRAK3 with the microglial marker IBA-1, the astrocyte marker GFAP, and the neuronal marker NeuN, indicating that IRAK3 was mainly

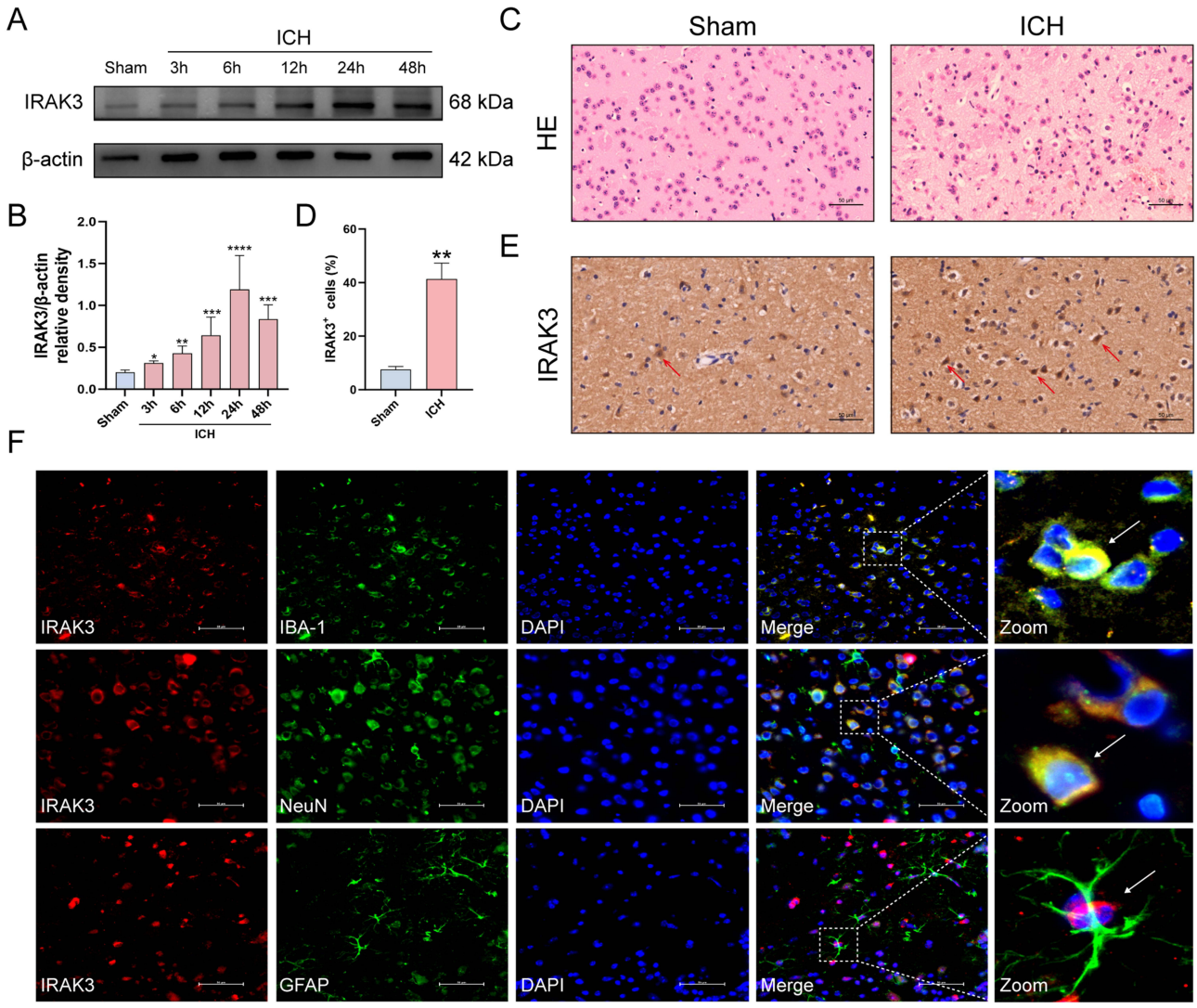

Figure 2 The expression and localization of IRAK3, and the tissue injury around the perihematomal area at different time points after ICH. (**A**) Representative Western blot bands of IRAK3. (**B**) Quantitative analysis of IRAK3 protein expression. (**C**) Representative HE staining images of the perihematomal tissue. Scale bar= 50 μm. (**D**) Quantitative analysis of IRAK3 positive cells in immunohistochemistry. (**E**) IRAK3 immunohistochemical staining images around the perihematomal tissue, with red arrows indicating representative IRAK3-positive cells. Scale bar= 50 μm. (**F**) Representative immunofluorescence images of IRAK3 (red), IBA-1 (green), NeuN (green) and GFAP (green) around the perihematomal tissue. Scale bar= 50 μm, n=3. *P<0.05, **P<0.01, ***P<0.001, ****P<0.0001 vs sham group.

https://doi.org/10.2147/JIR.S494611

expressed in microglia (Figure 2F). HE staining showed that the perihematomal tissue became loose, with obvious cell edema and vacuoles after ICH (Figure 2C).

Rh-IRAK3 Exacerbates Neurological Dysfunction and Neuroinflammation After ICH

The modified Garcia test, turning corner test, and forelimb placement test were used to assess neurological functional deficits with rh-IRAK3 treatment at 24 h and 72 h after ICH. The scores were significantly lower in the ICH group than sham group (Figure 3A–C). Compared to the ICH group, the scores continued to decrease in the ICH+rh-IRAK3 (3μg) group. However, there was no statistical difference between the rh-IRAK3 1 μg, rh-IRAK3 5 μg, and ICH + Vehicle groups (Figure 3A–C). Therefore, the optimal rh-IRAK3 dosage was determined to be 3 μg/μL. To assess the cytotoxic effects of rh-IRAK3 on BV2 microglia, a CCK-8 assay was conducted 24 hours after treatment with various concentrations of rh-IRAK3 (0, 1, 3, and 5 μg/mL). The results indicated that these concentrations of rh-IRAK3 did not exhibit cytotoxicity toward BV2 microglia cells (Figure 3D). To further evaluate the therapeutic efficacy of rh-IRAK3, neurological function assessments were performed 72 h after ICH. Consistently, treatment with rh-IRAK3 exacerbated the significant neurological impairment induced by ICH (Figure 3E–G). Western blotting was used to detect changes in inflammatory factors in perihematomal tissue. WB results showed that compared to the sham group, the ICH+Vehicle group had significantly increased levels of the inflammatory factors IL-1β, IL-18, IL-6 and TNF-α. Compared to the ICH +Vehicle group, rh-IRAK3 treatment continued to increase the expression of IL-1β, IL-18, IL-6 and TNF-α (Figure 3H–L).

DEG Identification and Enrichment Analysis After IRAK3 siRNA Treatment

To investigate the potential mechanisms by which IRAK3 promotes the inflammatory response and exacerbates neuronal injury after ICH, we used intracerebroventricular injection of IRAK3 siRNA to detect transcriptional changes, followed by RNA-seq analysis. We identified 1,797 differentially expressed genes in the IRAK3 siRNA-treated ICH group, with 783 upregulated and 1,014 downregulated genes (Figure 4A and B).

Gene Ontology (GO) enrichment analysis of DEGs revealed that IRAK3 was primarily involved in the regulation of inflammatory processes with red representing biological processes (BP), green indicating cellular components (CC), and blue denoting molecular functions (MF), such as (1) Regulation of inflammatory response and (2) Negative regulation of cytokine production. (3) Regulation of IL-18 and IL-1β production (Figure 4C). KEGG pathway enrichment analysis of the DEGs indicated that IRAK3 was involved in multiple functions, including (1) Cytokine-cytokine receptor interactions. (2) neuroactive ligand-receptor interactions. (3) NOD-like receptor and TNF signaling pathways. (3) NF-kappa B signaling pathway and IL-17 signaling pathways (Figure 4D).

To further explore the potential role of IRAK3 in the pathways following ICH, GSEA was performed. The GSEA results suggested that all six pro-inflammatory pathways were downregulated in the peri-hematoma brain tissue of mice treated with IRAK3 siRNA, as indicated by the peak values of the enrichment scores in the blue bars. In ICH mice with IRAK3 siRNA intracerebroventricular injection, the IL-17, NF-κB, TNF, and pro-inflammatory cytokine signaling pathways were suppressed. Additionally, there were downregulatory effects on other pathways, such as the cytosolic DNA sensing pathway, apoptosis, and necroptosis, in which IRAK3 plays a role. In summary, these analyses provide preliminary evidence for various potential mechanisms by which IRAK3 siRNA inhibits the inflammatory response after ICH (Figure 5A–I).

Knockdown IRAK3 Alleviates Short-Term and Long-Term Neurological Dysfunction After ICH

We further explored the role of IRAK3 in neurological dysfunction and neuroinflammation following ICH. First, qRT-PCR was used to detect the mRNA levels of IRAK3 at 24 hours after ICH in the 1, 2, and 3 μg/μL IRAK3 siRNA concentration groups. These results suggested that 2 μg/μL IRAK3 siRNA had the best knockdown effect. This concentration was used for qRT-PCR and the subsequent experiments (Figure 6A). We then evaluated neurological deficits using the modified Garcia, forelimb placement, and corner tests. Western blotting was performed to measure the

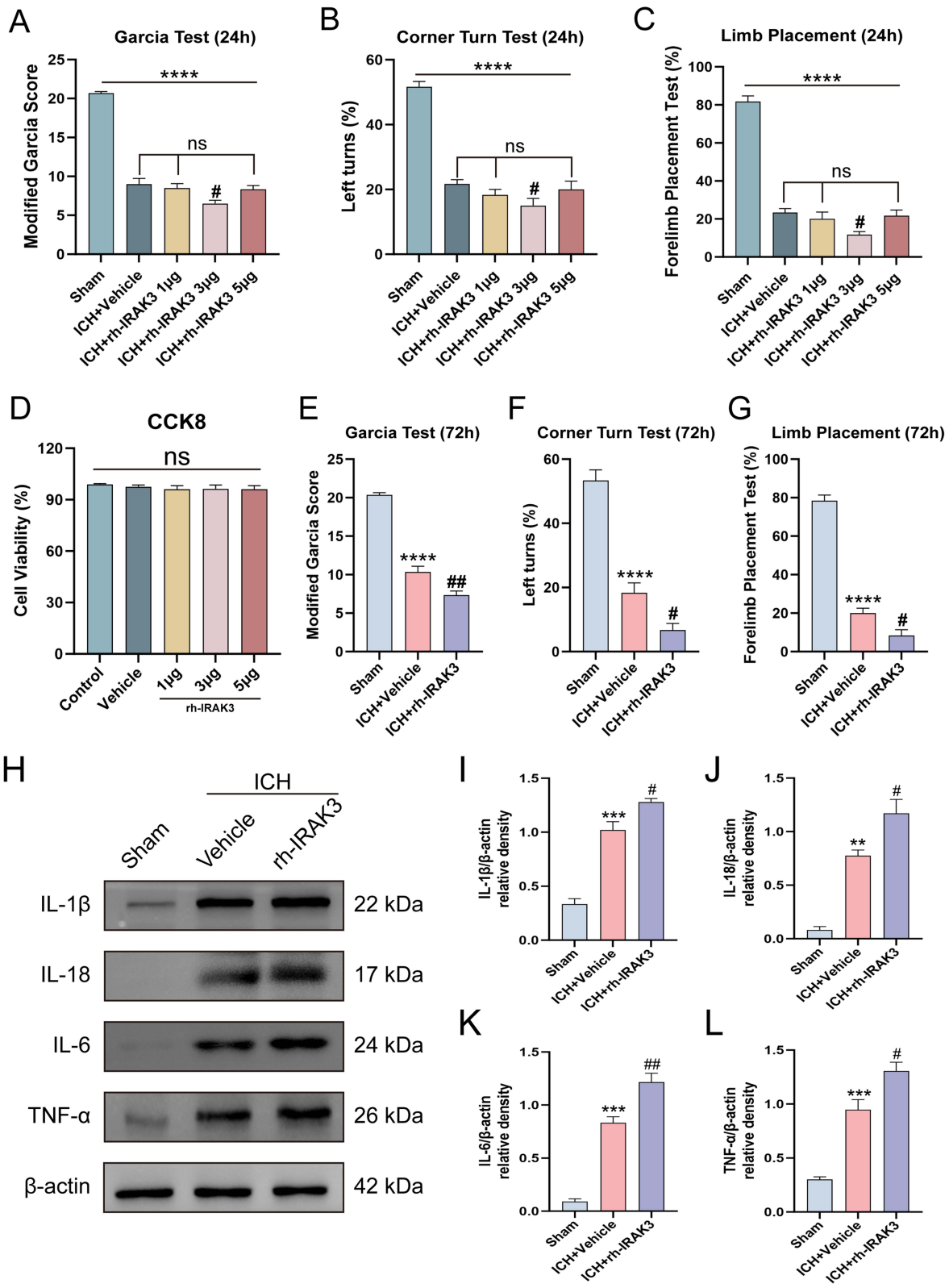

Figure 3 Rh-IRAK3 treatment exacerbated neurological dysfunction at 24 h and 72 h and decreased inflammatory response after ICH. (**A** and **E**) The modified Garcia test scores at 24 h and 72 h after ICH, n=6. (**B** and **F**) The left corner turning test scores at 24 h and 72 h after ICH, n=6. (**C** and **G**) The forelimb placement test scores at 24 h and 72 h after ICH, n=6. (**D**) CCK-8 Assay of BV2 cell viability after treatment with different concentrations of rh-IRAK3, n=6. (**H**) Representative Western blot bands of IL-1β, IL-18, IL-6 and TNF-α. (**I-L**) Quantitative analysis of IL-1β, IL-18, IL-6 and TNF-α protein expression, n=3. **P<0.01, ***P<0.001, ****P<0.0001 vs sham; #P<0.05, ##P<0.01 vs ICH+ Vehicle group.

https://doi.org/10.2147/JIR.S494611

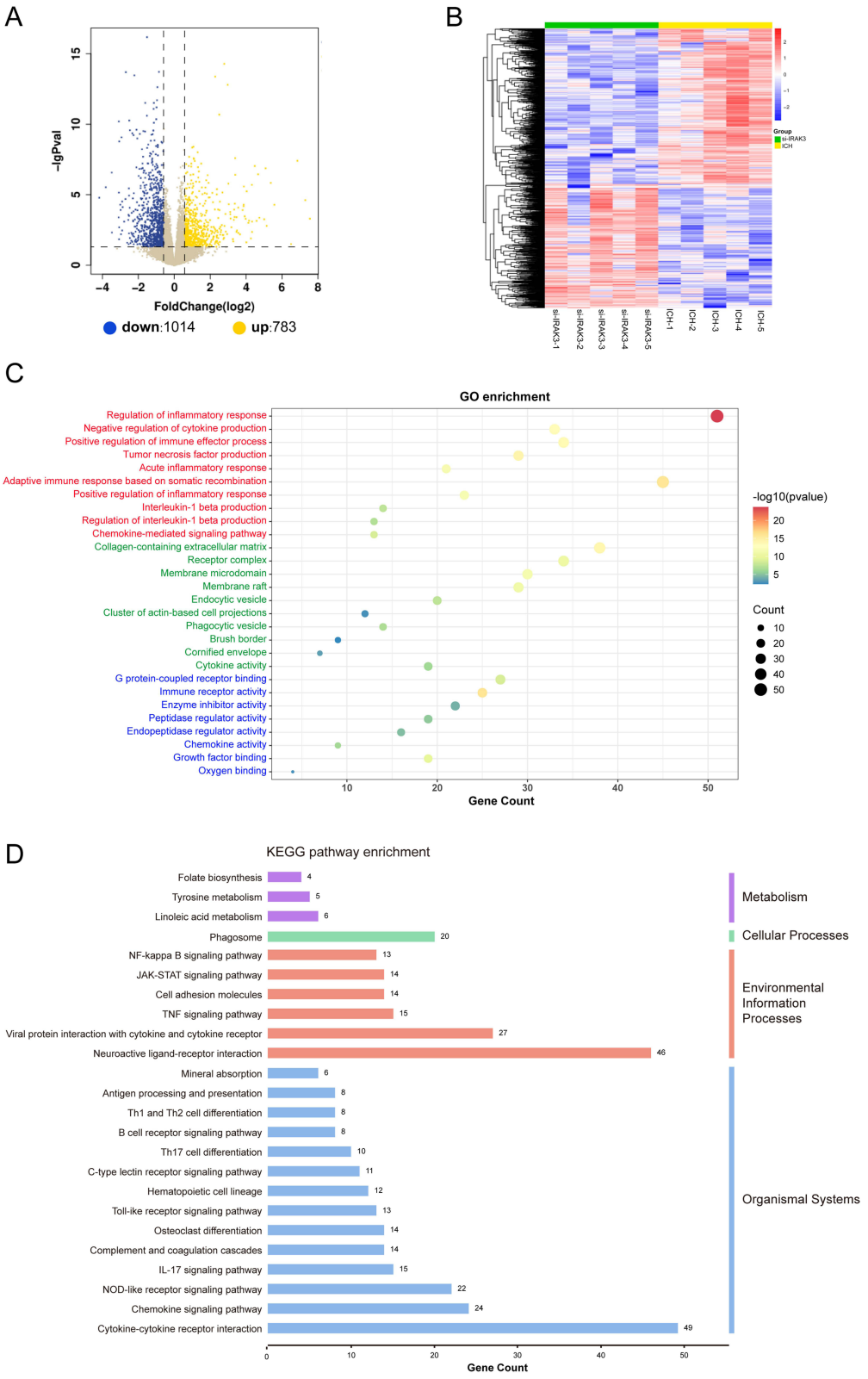

Figure 4 Differential expression gene and functional enrichment analysis of the ICH group and ICH+IRAK3 siRNA group. (**A**) Volcano plot of DEGs between ICH group and ICH+ siIRAK3. (**B**) Heatmap of differentially expressed genes between the ICH group and ICH+IRAK3 siRNA group. Upregulated genes are represented in yellow, and downregulated genes are denoted in blue. (**C**) GO enrichment analysis of DEGs, including biological processes (BP, red), cellular components (CC, green), and molecular functions (MF, blue). (**D**) KEGG pathway analysis of DEGs. The bar chart represents the count of genes annotated to each pathway. All pathway with p-value < 0.05.

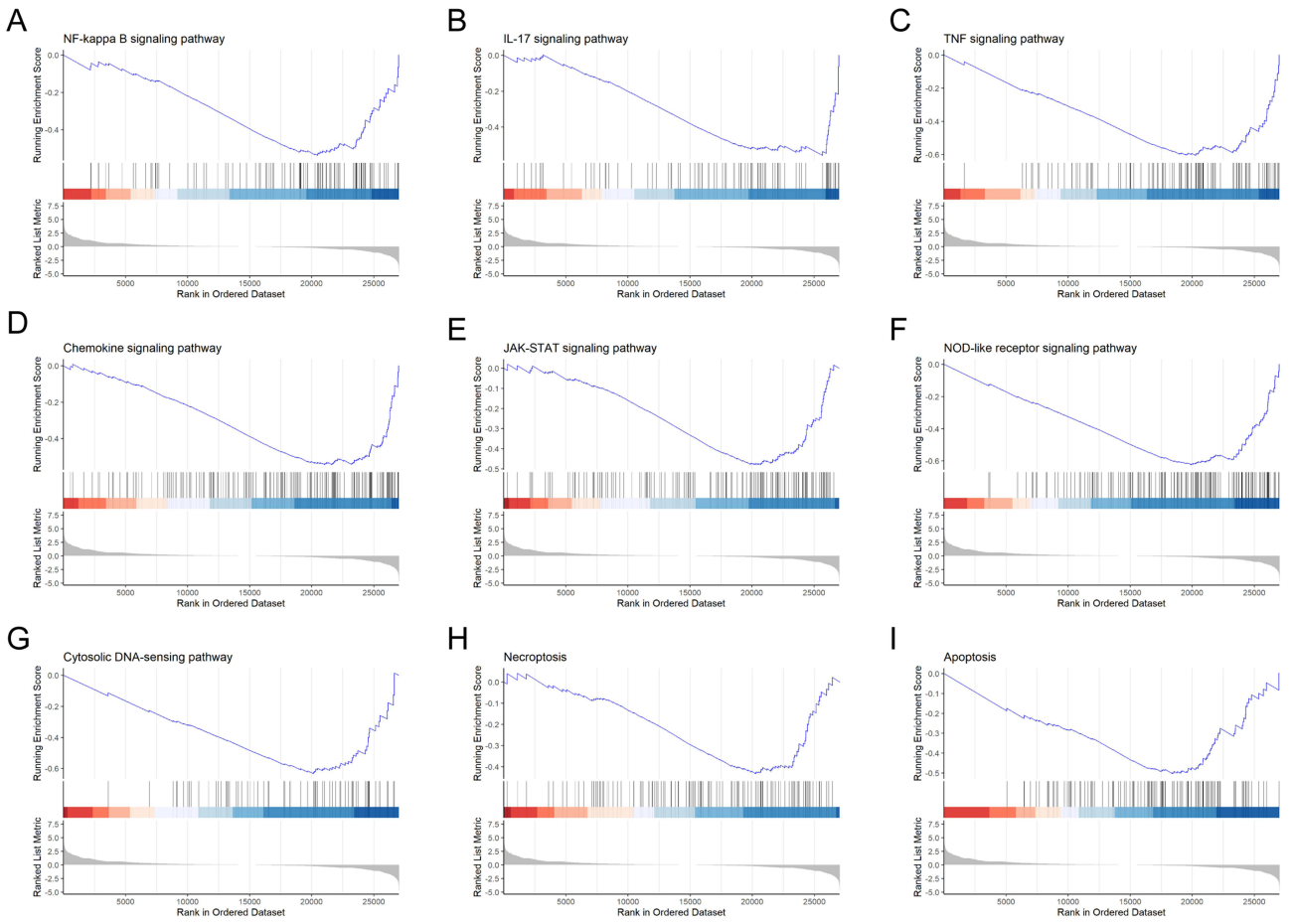

Figure 5 GSEA enrichment analysis. (**A**) NF-kappa B signaling pathway. (**B**) IL-17 signaling pathway. (**C**) TNF signaling pathway. (**D**) Chemokine signaling pathway. (**E**) JAK-STAT signaling pathway. (**F**) NOD-like receptor signaling pathway. (**G**) Cytosolic DNA-sensing pathway. (**H**) Necroptosis. (**I**) Apoptosis.

levels of proinflammatory cytokines. Compared to the sham group, the ICH group showed significantly lower neurological function scores. In contrast, the ICH+IRAK3 siRNA group exhibited significantly improved neurological function compared to the ICH group (Figure 6B–D). To assess the cytotoxic effects of IRAK3 siRNA on BV2 microglia, a CCK-8 assay was conducted 24 hours after treatment with various concentrations of IRAK3 siRNA (0, 1, 2, and 3 μg/mL). The results indicated that these concentrations of IRAK3 siRNA did not exhibit cytotoxicity toward BV2 microglia cells (Figure 6E). To further evaluate the therapeutic efficacy of IRAK3 siRNA, neurological function assessments were performed 72 h after ICH. Consistently, treatment with IRAK3 siRNA improved the significant neurological deficits induced by ICH (Figure 6F–H). The Morris water maze test was employed to assess the number of platform crossings, escape latency, and the duration of time spent in the target quadrant, in order to evaluate the effects of IRAK3 siRNA treatment on the recovery of spatial learning and memory function following ICH. Compared to the sham group, mice in the ICH + Vehicle group exhibited significant neurological deficits. However, the IRAK3 siRNA treatment group demonstrated a marked improvement in memory and learning abilities compared to the Vehicle group, as evidenced by a significant reduction in escape latency, an increased number of platform crossings, and a longer duration spent in the target quadrant (Figure 6I–L).

Knockdown IRAK3 Decreases Microglial Activation and Expression After ICH

Microglial activation is a key contributor to neuroinflammation following ICH. Immunofluorescence staining and Western blotting were used to detect changes in the microglia following ICH and IRAK3 siRNA treatment, respectively. The number of IBA-1-positive microglia markedly increased compared to sham group at 24 h after ICH. However, IRAK3 siRNA

https://doi.org/10.2147/JIR.S494611

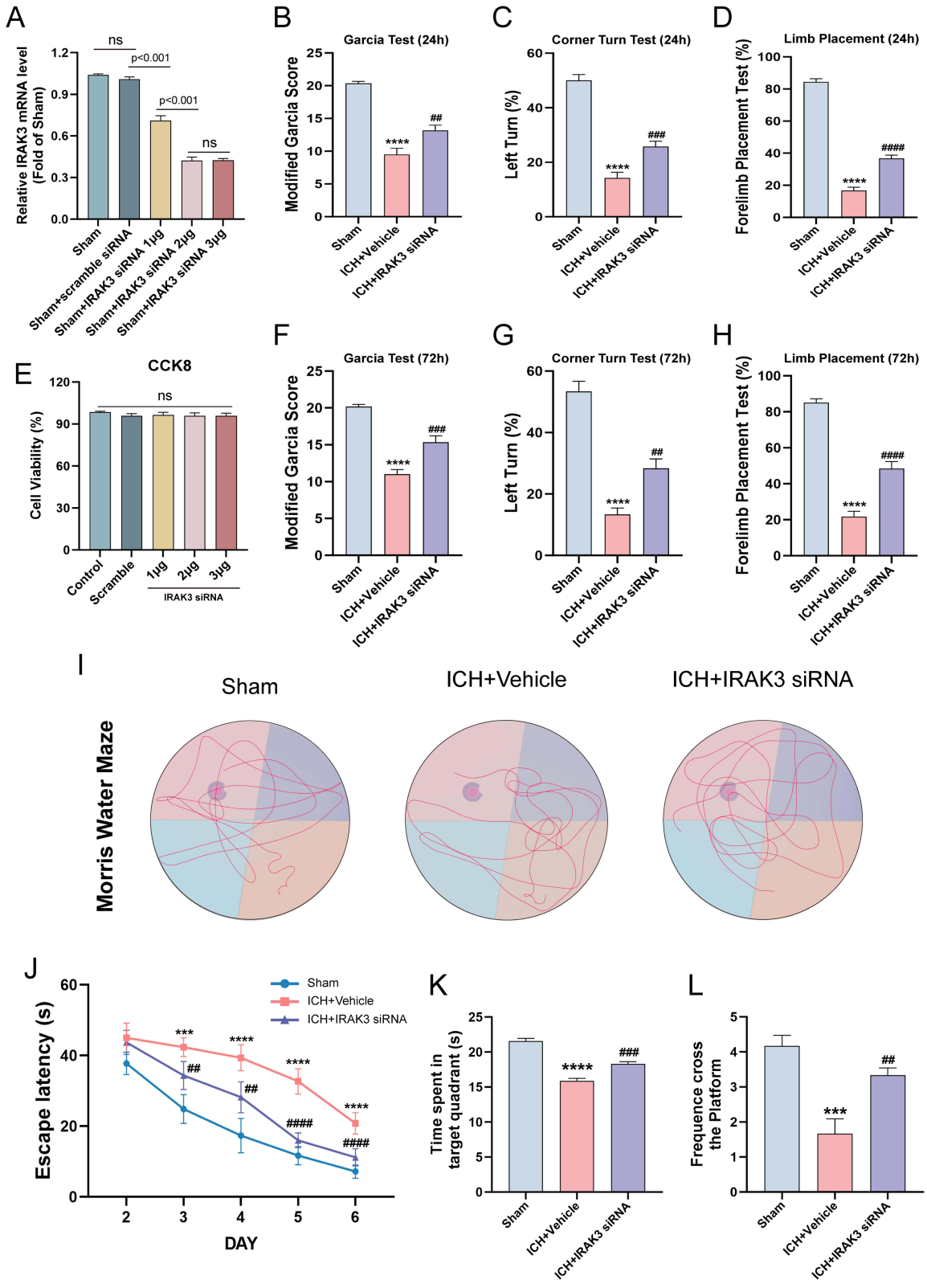

Figure 6 IRAK3 siRNA administration alleviated both short-term and long-term neurological dysfunction. (**A**) IRAK3 mRNA levels after treatment with different concentrations of IRAK3 siRNA, n=3. (**B and F**) The modified Garcia test at 24 h and 72 h after ICH, n=6. (**C and G**) The left corner turning test scores at 24 h and 72 h after ICH, n=6. (**D and H**) The forelimb placement test at 24 h and 72 h after ICH, n=6. (**E**) CCK-8 Assay of BV2 cell viability after treatment with different concentrations of rh-IRAK3, n=6. (**I**) Typical tracks of water maze exploration. (**J-L**) Escape latency, time spent in target quadrant and frequence cross the platform, n=6. ***P<0.001, ****P<0.0001 vs sham; ##P<0.01, ###P<0.001, ####P<0.0001 vs ICH+ Vehicle group.

treatment reduced the number of IBA-1-positive microglia compared to ICH+Vehicle group (Figure 7A and B). These findings suggest that IRAK3 knockdown decreases microglial activation after ICH. Western blotting revealed a substantial increase in the expression of IBA-1 in the ICH group compared to that in the sham group. However, after IRAK3 siRNA treatment, the expression of IBA-1 was markedly reduced compared to ICH group (Figure 7C and D).

Knockdown IRAK3 Suppresses NF-κB/IL-17A Signaling Pathway and Neuroinflammation

To further explore the mechanism by which IRAK3 participates in the inflammatory response, we used qRT-PCR, immunofluorescence, immunohistochemistry, and Western blotting to detect changes of IRAK3, IL-17A, NF-κB and pro-inflammatory factors levels in Sham, ICH and ICH+IRAK3 siRNA group. The results of qRT-PCR show that compared to the Sham group, the IRAK3 mRNA levels and the inflammatory cytokines IL-1β, IL-18, IL-6, and TNF-α mRNA levels were significantly elevated in the ICH+Vehicle group. In contrast, the IRAK3, IL-1β, IL-18, IL-6, and TNF-α mRNA levels were significantly reduced in the ICH+IRAK3 siRNA group compared to the ICH+Vehicle group (Figure 8A–E). Western blot analysis of perihematomal tissue from the ICH group revealed that, the proteins expression of IRAK3, IL-17A, NF-κB, IL-1β, IL-18, IL-6 and TNF-α was significantly higher in the ICH group than in the sham group. In contrast, ICH mice with IRAK3 siRNA treatment showed a marked reduction in IRAK3, IL-17A, NF-κB, IL-1β, IL-18, IL-6 and TNF-α expression compared to ICH+Vehicle group (Figure 8F–N). Double immunofluorescence staining of IBA-1 and IL-17A showed that IL-17A was expressed in microglia. Compared to the sham group, the proportion of IL-17A positive microglia was markedly increased in the ICH+Vehicle group. However, ICH mice with IRAK3 siRNA treatment showed a significant decrease in the proportion of IL-17A-positive microglia compared to the

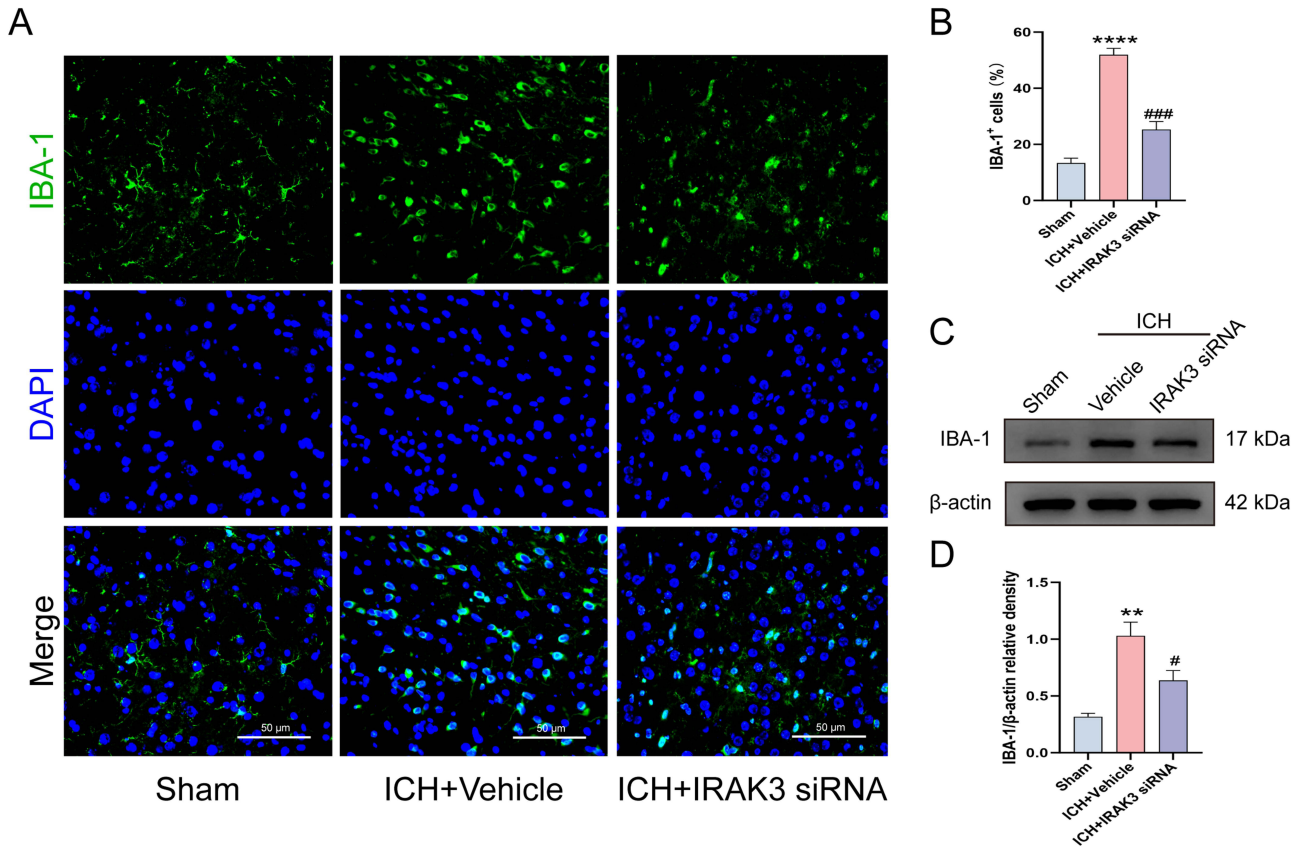

Figure 7 Knockdown of IRAK3 attenuated the activation of microglia following ICH. (**A**) Representative immunofluorescence images of the microglia 24 hours after ICH. Scale bar = 50 μm. (**B**) The percentage of IBA-1 positive microglial cells within the image of view. (**C**) Representative Western blot bands of IBA-1. (**D**) Quantitative analysis of IBA-1 protein expression, n=3. **P<0.01, ****P<0.0001 vs sham; #P<0.05, ###P<0.001 vs ICH+ Vehicle group.

https://doi.org/10.2147/JIR.S494611

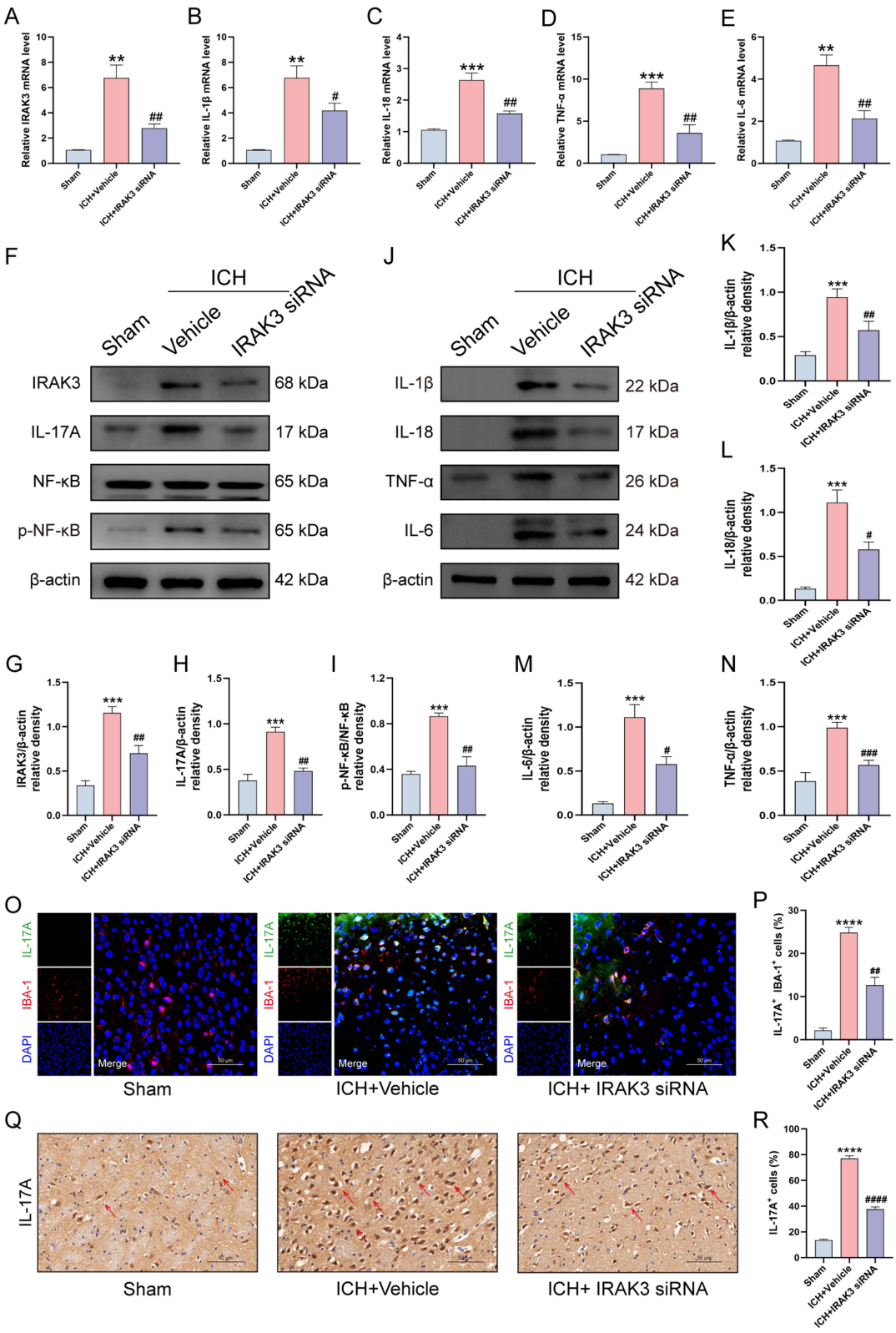

Figure 8 Inhibition IRAK3 suppressed the expression of the NF-κB/IL-17A signaling pathway and neuroinflammation after ICH. (**A-E**) Quantification of IRAK3, IL-1β, IL-18, and TNF-α relative mRNA level, n=3. (**F-N**) Representative Western blot bands and quantitative analysis of IRAK3, IL-17A, NF-κB, IL-1β, IL-18, IL-6 and TNF-α, n=3. (**O**) Immunofluorescent co-localization images of IBA-1 (red) and IL-17A (green). Scale bar = 50 μm. (**P**) Quantification of IBA-1-positive and IL-17A-positive cells, n=3. (**Q**) Representative immunohistochemical images of IL-17A in perihematomal tissue, with red arrows indicating representative IL17A-positive cells. Scale bar = 50 μm. (**R**) Quantification of IL-17A-positive cells by immunohistochemistry, n=3. **P<0.01, ***P<0.001, ****P<0.0001 vs sham; #P<0.05, ##P<0.01, ###P<0.001, #####P<0.0001 vs ICH+ Vehicle group.

ICH+Vehicle group (Figure 8O and P). Immunohistochemical staining of IL-17A in the perihematomal tissue showed that compared to the sham group, the expression of IL-17A in the brain tissue of the ICH+Vehicle group was significantly increased. However, the ICH group with IRAK3 siRNA treatment exhibited a significant decrease in IL-17A-positive microglia compared to the ICH+Vehicle group (Figure 8Q and R).

Effects of IRAK3 on pro-inflammatory factors after recombinant IL-17A intervention in vivo and vitro experiment.

To further investigate the mechanism by which IRAK3 regulates microglial-mediated neuroinflammation after ICH, we conducted intracerebroventricular injections of IRAK3 siRNA, followed by interventions using recombinant IL-17A. WB was used to analyze the expression levels of IL-17A, NF-κB, IL-1β, IL-18, IL-6 and TNF-α. The results show that, compared to the sham group, the ICH + vehicle group exhibited a significant upregulation of IL-17A, NF-κB, IL-1β, IL-18, IL-6, and TNF-α protein expression. In contrast, the ICH + IRAK3 siRNA group showed a significant decrease in the expression of IL-17A, NF-κB, IL-1β, IL-18, IL-6, and TNF-α compared to the ICH + vehicle group. However, in the ICH + IL-17A + vehicle group, the expression levels of IL-17A, NF-κB, IL-1β, IL-18, IL-6, and TNF-α were further increased compared to ICH+vehicle group. Compared to the ICH + IL-17A + vehicle group, the ICH + IL-17A + IRAK3 siRNA group had a significantly reduced expression of IL-17A, NF-κB, IL-1β, IL-18, IL-6, and TNF-α. Meanwhile, ELISA was used to measure changes in the inflammatory factors IL-1β and TNF-α in perihematomal brain tissue after ICH for 24 hours. The results of the ELISA for IL-1β and TNF-α were consistent with the trends observed in the Western blot results for IL-1β and TNF-α (Figure 9A–I). To further explore whether knockdown IRAK3 reduced microglial-mediated neuroinflammation through the NF-κB/IL-17A signaling pathway and pro-inflammatory factors IL-1β, IL-18, IL-6 and TNF-α, we cultured BV2 microglial cells in vitro and stimulated them with LPS while intervening with IRAK3 siRNA and recombinant IL-17A. WB was used to assess the changes in IL-17A, NF-κB, IL-1β, IL-18, IL-6 and TNF-α, and ELISA was used to assess the expression of IL-1β and TNF-α at 24 h after ICH. The results show that in vitro experiments involved WB analysis to assess changes in the protein expression of IL-17A, NF-κB, IL-1β, IL-18, IL-6, and TNF-α. Additionally, ELISA was used to measure changes in IL-1β and TNF-α, and the trends observed were consistent with the results obtained from in the vivo experiments (Figure 9J–R).

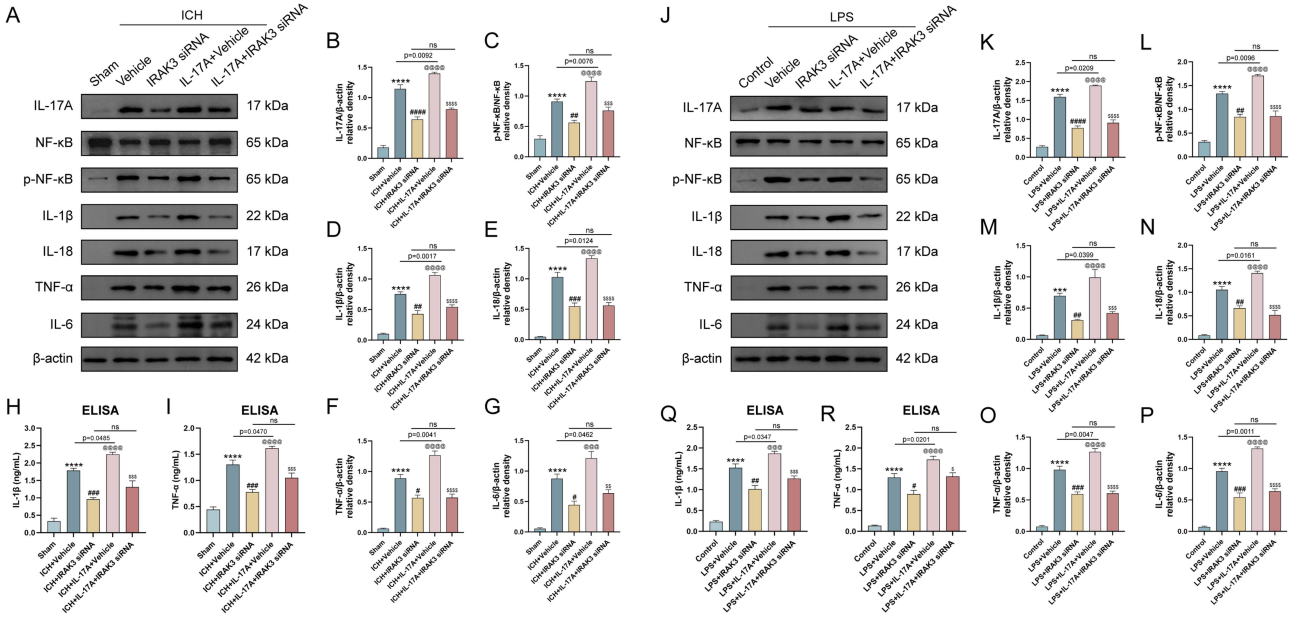

Figure 9 Inhibition IRAK3 decreased microglial neuroinflammation via NF-κB/IL-17A pathway in vivo and vitro. (**A**) Representative Western blot bands of IL-17A and NF-κB after ICH. (**B-G**) Quantitative analysis of Western blot of IL-17A, NF-κB, IL-1β, IL-18, IL-6 and TNF-α at 24 h after ICH, n=3. (**H and I**) ELISA analysis of inflammatory factors IL-1β and TNF-α in the perihematomal tissue 24 hours after ICH, n=3. (**J**) Representative Western blot bands of IL-17A, NF-κB, IL-1β, IL-18, IL-6 and TNF-α in vitro experiment. (**K-P**) Quantitative analysis of Western blot of IL-17A, NF-κB, IL-1β, IL-18, IL-6 and TNF-α in vitro experiment, n=3. (**Q and R**) ELISA analysis of pro-inflammatory factors IL-1β and TNF-α expression 24 hours after LPS stimulation of BV2 microglia, n=3. ***P<0.001, ****P<0.0001 vs Sham/Control; #P<0.05, ##P<0.01, ###P<0.001, ####P<0.0001 vs ICH/LPS+ Vehicle group. @@@ P<0.001, @@@@ P<0.0001 vs ICH/LPS+IRAK3 siRNA group; $ P<0.05, $$ P<0.01, $$$ P<0.001, $$$$ P<0.0001 vs ICH/LPS+ IL-17A+Vehicle group.

https://doi.org/10.2147/JIR.S494611

Discussion

This study investigated the role and mechanism of IRAK3 in an experimental mouse model of ICH, in which IRAK3 affects neuroinflammation. Our results were as follows: (1) The expression of IRAK3 a time-dependently manner after ICH, peaking at 24 h and declining at 48 h. Immunofluorescence co-localization showed that IRAK3 was mainly expressed in microglia. (2) Activation IRAK3 exacerbated neuroinflammatory response. (3) Intracerebroventricular injection of IRAK3 siRNA downregulated inflammatory pathways. (4) IRAK3 knockdown improved both short-term and long-term neurological functional deficits, accompanied by decreased expression of NF-κB/IL-17A signaling pathway and inflammatory factors. (5) Knockdown of IRAK3 can reverse the pro-inflammatory process induced by recombinant IL-17A in vivo and in vitro. Overall, our results demonstrate that IRAK3 levels were significantly upregulated after ICH. IRAK3 is expressed in microglia. Knockdown of IRAK3 decreased neuroinflammation around hematoma tissue and improved both short-term and long-term neurological deficits after ICH, at least in part, by suppressing the NF-κB/IL-17A signaling pathway (Figure 10).

Secondary brain injury following intracerebral hemorrhage is a comprehensive result of a series of adverse reactions, of which neuroinflammation is a crucial step in this process.[29,36] Specifically, blood breakdown products activate microglia, leading to increased transcription and expression of inflammatory factors, which in turn triggers an inflammatory storm around the hematoma.[37,38] Previous studies have demonstrated a significant increase in the levels of TNF-α and IL-1β in both the perihematomal region and serum, which can serve as critical indicators of neuroinflammation during the acute phase of ICH.[39,40] Reducing the levels of inflammatory factors after intracerebral hemorrhage can improve the neurological deficits.[36] This study found that in the acute phase of ICH, the levels of inflammatory factors IL-1β, IL-18, TNF-α and IL-6 in the perihematomal tissue were significantly increased, consistent with previous researches. Furthermore, our study indicates that knockdown of IRAK3 resulted in a reduction of inflammatory factors surrounding the hematoma. This suggests that inhibition of IRAK3 during the acute phase after ICH can attenuate the amplification of neuroinflammatory signaling. Therefore, targeting IRAK3 may represent an effective strategy for decreasing secondary brain injury following ICH; however, specific inhibitors of IRAK3 have not yet been exploited. This study contributes to investigate the role and molecular mechanisms of IRAK3 inhibition in decreasing microglia-mediated neuroinflammatory responses after ICH, providing a promising therapeutic strategy for ICH.

IRAK3, a member of the IRAK family, also known as IRAKM, was initially characterized for its regulatory role in TLR signaling and NF-κB pathway activation, subsequently modulating the inflammatory response.[14,41] IRAK3 has been identified as a crucial regulator of inflammation in various disease contexts, including chronic alcoholic liver disease, asthma, and myocardial ischemia-reperfusion injury.[42–44] In CNS diseases, such as cerebral ischemia and subarachnoid hemorrhage, IRAK3 has been considered to have neuroprotective properties. Lyu C et al demonstrated that in a mouse tMCAO disease model, IRAK3 mRNA levels peaked at 1 hour after ischemia and subsequently declined, reaching a minimal level at 24 hours. Conversely, IRAK3 knockout was associated with increased infarct volume, blood-brain barrier permeability, and inflammatory response levels[15]. However, our data indicate that IRAK3 expression increased gradually after ICH, peaking at 24 hours and then declining at 48 hours. Interestingly, our findings contradict those of previous studies on cerebral ischemia, where neuronal damage is primarily induced by ischemia-hypoxia.[45] In contrast, brain damage following ICH is mainly attributed to secondary insults triggered by hemoglobin degradation products.[46] Furthermore, Cao C et al found that in a mouse subarachnoid hemorrhage (SAH) disease model, TREM2 mitigated neuroinflammation and exerted neuroprotective effects by activation IRAK3 expression.[47] In this study, IRAK3 protein levels were found to be higher after SAH compared to the sham group, consistent with our research findings. However, Cao C et al only investigated IRAK3 expression at 48 hours post-SAH, without examining the temporal dynamics of IRAK3 expression in the SAH disease model. Moreover, the study focused on the basal cortical region, whereas our research was conducted in the striatum. Although both ICH and SAH involve secondary brain injury triggered by hemoglobin degradation products, the underlying pathophysiological mechanisms differ between the two conditions.[48] Notably, IRAK3 does not uniformly function as an inhibitor of inflammation, as evidenced by a study by Zhang et al in the experimental autoimmune encephalomyelitis (EAE) disease model. In this study, IRAK3 was shown to promote neuroinflammation by activating the caspase-8-mediated inflammasome in microglia, highlighting the necessity of IRAK3 for the activation of inflammatory signaling in microglia.[17] In summary, IRAK3 plays a crucial role in the

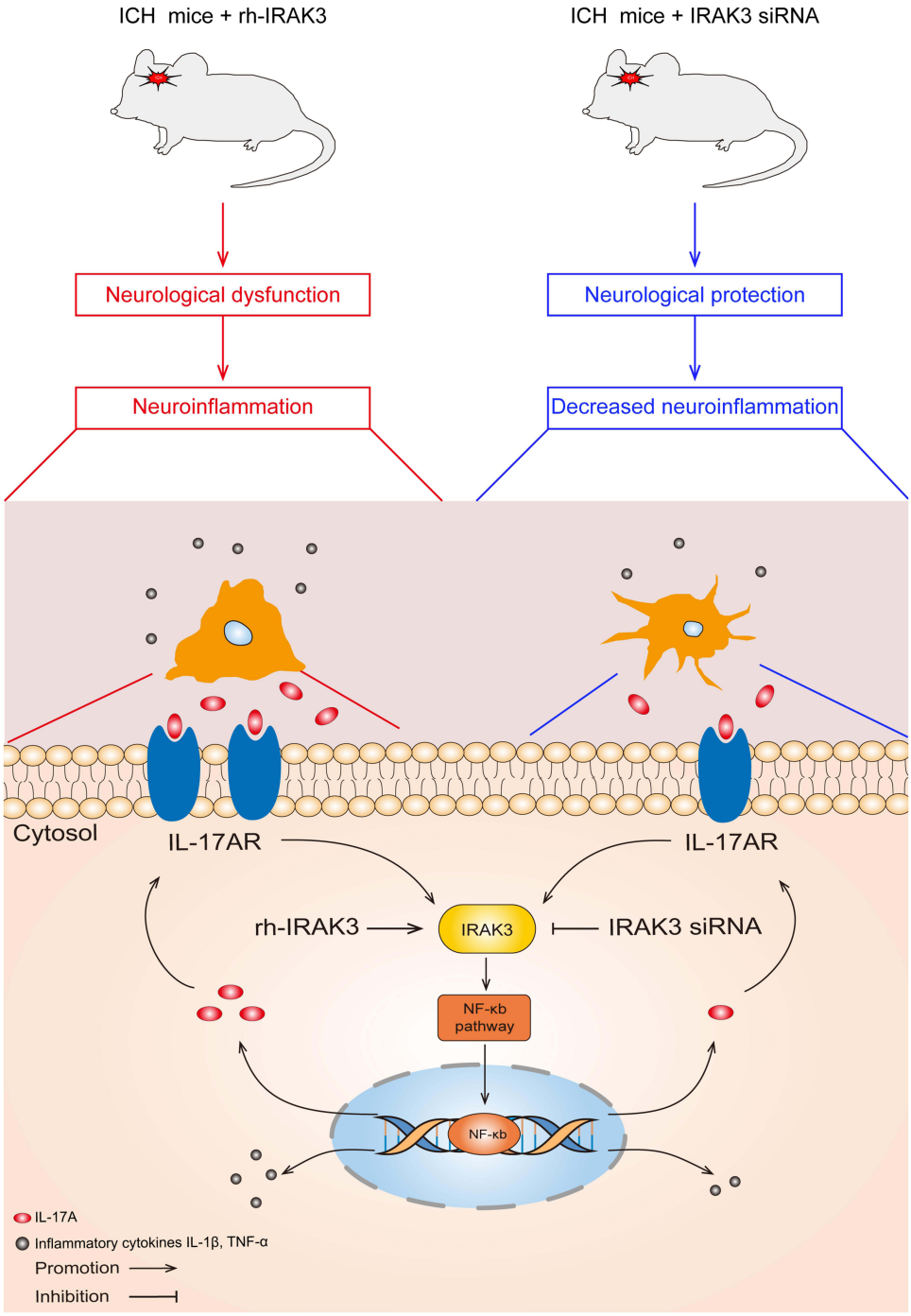

Figure 10 Schematic Illustration of the Mechanism. IRAK3 activation aggravates neurological dysfunction and increased neuroinflammation in the perihematomal region following ICH. Knockdown of IRAK3 improved both short-term and long-term neurological dysfunction and decreased neuroinflammation, and this is partly mediated via the NF-κB/IL-17A signaling pathway.

central nervous system, and the differential expression and function of IRAK3 may be attributed to varying disease contexts or system. Currently, the role of IRAK3 in ICH remains unclear. Therefore, investigating the function of IRAK3 in ICH is warranted, and it may potentially serve as a therapeutic target for treating ICH. Our study reveals that exogenous IRAK3 enhanced inflammatory factor expression, whereas knockdown IRAK3 reduced inflammatory factor expression and alleviated short-term and long-term neurological dysfunction. These findings expand our understanding of IRAK3's regulatory mechanisms in the pathogenesis of central nervous system diseases. In clinical translation, the development of IRAK3

https://doi.org/10.2147/JIR.S494611

inhibitors or RNA interference technologies to suppress its overactivation can enable precise treatment, while dynamic monitoring of IRAK3 expression could optimize the therapeutic window and personalize treatment strategies. Furthermore, high IRAK3 levels may serve as a molecular biomarker for poor prognosis in the acute phase of ICH patients.

IL-17A is one of the main members of the IL-17 family and primarily exerts its effects by interacting with IL-17R, which significantly enhancing inflammatory responses.[49] IL-17A is involved in various CNS inflammatory diseases and plays a crucial role in microglial cells.[50] Previous studies have shown that activated microglial cells secrete IL-1β, which promotes the secretion of IL-17A, while IL-17A, in turn enhances the secretion of IL-1β from microglial cells, creating a vicious cycle of inflammatory storms.[51] Furthermore, research has shown that inhibiting the NF-κB/IL-17A signaling pathway can reduce neuroinflammatory responses after ICH, improve neurological function, and increase survival rates in ICH mice.[52] In our study, we performed RNA-seq on the perihematomal region of IRAK3 knockdown ICH mice and enriched KEGG and GSEA, including NF-κB/IL-17 signaling. These sequencing results are consistent with previous studies. Additionally, we treated ICH mice with exogenous recombinant IL-17A and observed increased expression of inflammatory factors compared to the ICH group. Knockdown of IRAK3 mitigated this process and reduced NF-κB/IL-17A signal transduction. Thus, IRAK3 partly targets post-ICH neuroinflammation by regulating the NF-κB/IL-17A signaling pathway.

In conclusion, this study suggests that IRAK3 plays a functional role in regulating inflammatory signaling pathways and is critical for attenuating neuroinflammation after ICH. IRAK3 exacerbates the neuroinflammatory response in perihematomal tissue via activation of the NF-κB/IL-17A signaling pathway, which in turn worsens neurological deficits after ICH in mice. Therefore, targeting IRAK3 may represent a potential therapeutic strategy to mitigate secondary brain injury after ICH.

This study has several limitations. First, following IRAK3 knockdown in ICH mice, multiple inflammatory pathways were downregulated, but we only focused on the relationship between IRAK3 and the NF-κB/IL-17A signaling pathway. Further investigation is warranted to determine whether IRAK3 interacts with other inflammatory pathways to reduce neuroinflammation. Second, to minimize the influence of estrogen on ICH, our study only used male mice. Therefore, the role of IRAK3 in female mice remains to be explored.[53] Third, astrocytes are also key cells that induce neuroinflammation, and it is worth investigating how IRAK3 regulates astrocyte-induced inflammatory responses.[37] Finally, we did not examine IRAK3 expression in neurons, and whether IRAK3 can directly regulate neuronal processes remains to be further investigated, leaving this as a promising area for future research.

Conclusion

Our study indicates that the activation of IRAK3 exacerbated SBI following ICH. In contrast, suppression of IRAK3 expression ameliorated the neuroinflammatory response in perihematomal tissue and improved short-term and long-term neurological deficits, partially through modulation of the NF-κB/IL-17A signaling pathway. However, further studies are needed to investigate the role of IRAK3 in modulating other inflammatory pathways and its role in neurons and astrocytes. Exploring IRAK3 inhibitors may be a promising therapeutic approach for the treatment of ICH.

Abbreviations

IRAK3: Interleukin-1 receptor-associated kinase-3; IL, interleukin; ICH, intracerebral hemorrhage; CNS, central nervous system; KEGG, Kyoto Encyclopedia of Genes and Genomes; WB, Western blot; HE, hematoxylin and eosin; IBA-1, ionized calcium-binding adaptor molecule; GFAP, glial fibrillary acidic protein; qRT-PCR, quantitative real-time polymerase chain reaction; GO, gene ontology; DEG, differentially expressed genes; SBI, secondary brain injury; IHC, immunohistochemistry; IF, immunofluorescence.

Data Sharing Statement

All the data used in this study are available from the corresponding author upon reasonable request.

Ethics approval and consent to participate

All animal studies were approved by the Ethics Committee of Zhujiang Hospital of Southern Medical University (Animal Ethics No. LAEC-2023-156) and complied with the guidelines of the National Institute of Health.

Acknowledgments

We would like to thank the staff at the Central Laboratory of Zhujiang Hospital and the Southern Medical University.

Author Contributions

All authors made a significant contribution to the work reported, whether that is in the conception, study design, execution, acquisition of data, analysis and interpretation, or in all these areas; took part in drafting, revising or critically reviewing the article; gave final approval of the version to be published; have agreed on the journal to which the article has been submitted; and agree to be accountable for all aspects of the work.

Funding

This work was supported by grants from the National Key R&D Program of China (2022YFA1104900), Key Science and Technology Project of Guangdong (No. 2023B1111050004), and Key Projects of Health Collaborative Innovation of Guangzhou (No. 201803040016) to Prof. Xiaodan JIANG.

Disclosure

The authors declare no conflicts of interest in this work.

References

1. Puy L, Parry-Jones AR, Sandset EC, et al. Intracerebral haemorrhage. *Nat Rev Dis Primers*. 2023;9(1):14. doi:10.1038/s41572-023-00424-7
2. Li X, Wang T, Zhang D, et al. Andrographolide ameliorates intracerebral hemorrhage induced secondary brain injury by inhibiting neuroinflammation induction. *Neuropharmacology*. 2018;141:305–315. doi:10.1016/j.neuropharm.2018.09.015
3. Gao X, Li R, Luo L, et al. Alpha-asarone ameliorates neurological deterioration of intracerebral hemorrhagic rats by alleviating secondary brain injury via anti-excitotoxicity pathways. *Phytomedicine*. 2022;105:154363. doi:10.1016/j.phymed.2022.154363
4. Babu R, Bagley JH, Di C, Friedman AH, Adamson C, Thrombin and hemin as central factors in the mechanisms of intracerebral hemorrhage-induced secondary brain injury and as potential targets for intervention. *Neurosurg Focus*. 2012;32(4):E8. doi:10.3171/2012.1.FOCUS11366
5. Zhao X, Aronowski J, Nrf2 to pre-condition the brain against injury caused by products of hemolysis after ICH. *Transl Stroke Res*. 2013;4(1):71–75. doi:10.1007/s12975-012-0245-y
6. Bobinger T, Burkardt P, Bh H, Manaenko A, Programmed cell death after intracerebral hemorrhage. *Curr Neuropharmacol*. 2018;16(9):1267–1281. doi:10.2174/1570159X15666170602112851
7. Wang J, Preclinical and clinical research on inflammation after intracerebral hemorrhage. *Prog Neurobiol*. 2010;92(4):463–477. doi:10.1016/j.pneurobio.2010.08.001
8. Wang J, Dore S, Inflammation after intracerebral hemorrhage. *J Cereb Blood Flow Metab*. 2007;27(5):894–908. doi:10.1038/sj.jcbfm.9600403
9. Barichello T, Giridharan CCHR VV, Ritter C, Dal-Pizzol F, Neurochemical effects of sepsis on the brain. *Clin Sci*. 2023;137(6):401–414. doi:10.1042/CS20220549
10. Aronowski J, Zhao X, Molecular pathophysiology of cerebral hemorrhage: secondary brain injury. *Stroke*. 2011;42(6):1781–1786. doi:10.1161/STROKEAHA.110.596718
11. Keep RF, Hua Y, Xi G, Intracerebral haemorrhage: mechanisms of injury and therapeutic targets. *Lancet Neurol*. 2012;11(8):720–731. doi:10.1016/S1474-4422(12)70104-7
12. Nguyen TH, Axell A, Turek I, Wright B, Meehan-Andrews T, Irving HR, Modulation of inflammatory cytokine production in human monocytes by cGMP and IRAK3. *Int J Mol Sci*. 2022;23(5). doi:10.3390/ijms23052552
13. Janssens S, Beyaert R, Functional diversity and regulation of different interleukin-1 receptor-associated kinase (IRAK) family members. *Mol Cell*. 2003;11(2):293–302. doi:10.1016/s1097-2765(03)00053-4
14. Kobayashi K, Hernandez LD, Galan JE, Janeway CA Jr, Medzhitov R, Flavell RA, IRAK-M is a negative regulator of Toll-like receptor signaling. *Cell*. 2002;110(2):191–202. doi:10.1016/s0092-8674(02)00827-9
15. Lyu C, Zhang Y, Gu M, et al. IRAK-M deficiency exacerbates ischemic neurovascular injuries in experimental stroke mice. *Front Cell Neurosci*. 2018;12:504. doi:10.3389/fncel.2018.00504
16. Oliveros G, Wallace CH, Chaudry O, et al. Repurposing ibudilast to mitigate alzheimer's disease by targeting inflammation. *Brain*. 2023;146(3):898–911. doi:10.1093/brain/awac136
17. Zhang CJ, Jiang M, Zhou H, et al. TLR-stimulated IRAKM activates caspase-8 inflammasome in microglia and promotes neuroinflammation. *J Clin Invest*. 2018;128(12):5399–5412. doi:10.1172/JCI121901
18. Liu Y, Zhang M, Lou L, et al. IRAK-M associates with susceptibility to adult-onset asthma and promotes chronic airway inflammation. *J Immunol*. 2019;202(3):899–911. doi:10.4049/jimmunol.1800712
19. Li J, Zheng Z, Liu Y, Zhang H, Zhang Y, Gao J, IRAK-M has effects in regulation of lung epithelial inflammation. *Respir Res*. 2023;24(1):103. doi:10.1186/s12931-023-02406-5
20. Gao L, Li PP, Shao TY, et al. Neurotoxic role of interleukin-17 in neural stem cell differentiation after intracerebral hemorrhage. *Neural Regen Res*. 2020;15(7):1350–1359. doi:10.4103/1673-5374.272614
21. Li Y, Tu H, Zhang S, et al. P2Y6 receptor activation aggravates NLRP3-dependent microglial pyroptosis via downregulation of the PI3K/AKT pathway in a mouse model of intracerebral hemorrhage. *Mol Neurobiol*. 2024;61(7):4259–4277. doi:10.1007/s12035-023-03834-6

22. Ye XC, Hao Q, Ma WJ, et al. Dectin-1/Syk signaling triggers neuroinflammation after ischemic stroke in mice. *J Neuroinflammation*. 2020;17(1):17. doi:10.1186/s12974-019-1693-z
23. Deng S, Chen X, Lei Q, Lu W, AQP2 promotes astrocyte activation by modulating the TLR4/NFkappaB-p65 pathway following intracerebral hemorrhage. *Front Immunol*. 2022;13:847360. doi:10.3389/fimmu.2022.847360
24. Yu H, Cao X, Li W, et al. Targeting connexin 43 provides anti-inflammatory effects after intracerebral hemorrhage injury by regulating YAP signaling. *J Neuroinflammation*. 2020;17(1):322. doi:10.1186/s12974-020-01978-z
25. Zeng J, Chen Y, Ding R, et al. Isoliquiritigenin alleviates early brain injury after experimental intracerebral hemorrhage via suppressing ROS- and/or NF-kappaB-mediated NLRP3 inflammasome activation by promoting Nrf2 antioxidant pathway. *J Neuroinflammation*. 2017;14(1):119. doi:10.1186/s12974-017-0895-5
26. Li R, Liu W, Yin J, et al. TSG-6 attenuates inflammation-induced brain injury via modulation of microglial polarization in SAH rats through the SOCS3/STAT3 pathway. *J Neuroinflammation*. 2018;15(1):231. doi:10.1186/s12974-018-1279-1
27. Ye B, Tao T, Zhao A, et al. Blockade of IL-17A/IL-17R pathway protected mice from sepsis-associated encephalopathy by inhibition of microglia activation. *Mediators Inflamm*. 2019;2019:8461725. doi:10.1155/2019/8461725
28. Ding Z, Zhong Z, Wang J, et al. Inhibition of dectin-1 alleviates neuroinflammatory injury by attenuating NLRP3 inflammasome-mediated pyroptosis after intracerebral hemorrhage in mice: preliminary study results. *J Inflamm Res*. 2022;15:5917–5933. doi:10.2147/JIR.S384020
29. Li Y, Tu H, Zhang S, et al. P2Y6 receptor activation aggravates NLRP3-dependent microglial pyroptosis via downregulation of the PI3K/AKT pathway in a mouse model of intracerebral hemorrhage. *Mol Neurobiol*. 2023;doi:10.1007/s12035-023-03834-6
30. Robinson MD, McCarthy DJ, Smyth GK. edgeR: a bioconductor package for differential expression analysis of digital gene expression data. *Bioinformatics*. 2010;26(1):139–140. doi:10.1093/bioinformatics/btp616
31. Bai C, Liu X, Wang F, et al. Identification of immune-related biomarkers for intracerebral hemorrhage diagnosis based on RNA sequencing and machine learning. *Front Immunol*. 2024;15:1421942. doi:10.3389/fimmu.2024.1421942
32. Lai Z, Li C, Ma H, et al. Hydroxysafflor yellow a confers neuroprotection against acute traumatic brain injury by modulating neuronal autophagy to inhibit NLRP3 inflammasomes. *J Ethnopharmacol*. 2023;308:116268. doi:10.1016/j.jep.2023.116268
33. Gao M, Song Y, Liu Y, Miao Y, Guo Y, Chai H, TNF-alpha/TNFR1 activated astrocytes exacerbate depression-like behavior in CUMS mice. *Cell Death Discov*. 2024;10(1):220. doi:10.1038/s41420-024-01987-4
34. Guo C, Zhou X, Wang X, et al. Annao Pingchong decoction alleviate the neurological impairment by attenuating neuroinflammation and apoptosis in intracerebral hemorrhage rats. *J Ethnopharmacol*. 2023;310:116298. doi:10.1016/j.jep.2023.116298
35. Ding M, Jin L, Wei B, et al. Tumor necrosis factor-stimulated gene-6 ameliorates early brain injury after subarachnoid hemorrhage by suppressing NLRC4 inflammasome-mediated astrocyte pyroptosis. *Neural Regen Res*. 2024;19(5):1064–1071. doi:10.4103/1673-5374.385311
36. Tschoe C, Bushnell CD, Duncan PW, Alexander-Miller MA, Wolfe SQ, Neuroinflammation after intracerebral hemorrhage and potential therapeutic targets. *J Stroke*. 2020;22(1):29–46. doi:10.5853/jos.2019.02236
37. Alsbrook DL, Di Napoli M, Bhatia K, et al. Neuroinflammation in acute ischemic and hemorrhagic stroke. *Curr Neurol Neurosci Rep*. 2023;23(8):407–431. doi:10.1007/s11910-023-01282-2
38. Lan X, Han X, Li Q, Yang QW, Wang J, Modulators of microglial activation and polarization after intracerebral haemorrhage. *Nat Rev Neurol*. 2017;13(7):420–433. doi:10.1038/nrneurol.2017.69
39. Gan H, Zhang L, Chen H, et al. The pivotal role of the NLRC4 inflammasome in neuroinflammation after intracerebral hemorrhage in rats. *Exp Mol Med*. 2021;53(11):1807–1818. doi:10.1038/s12276-021-00702-y
40. Luo J, Chen Y, Tang G, et al. Gut microbiota composition reflects disease progression, severity and outcome, and dysfunctional immune responses in patients with hypertensive intracerebral hemorrhage. *Front Immunol*. 2022;13:869846. doi:10.3389/fimmu.2022.869846
41. Zhou H, Yu M, Fukuda K, et al. IRAK-M mediates Toll-like receptor/IL-1R-induced NFkappaB activation and cytokine production. *EMBO J*. 2013;32(4):583–596. doi:10.1038/emboj.2013.2
42. Zhou H, Yu M, Zhao J, et al. IRAKM-Mincle axis links cell death to inflammation: pathophysiological implications for chronic alcoholic liver disease. *Hepatology*. 2016;64(6):1978–1993. doi:10.1002/hep.28811
43. Nechama M, Kwon J, Wei S, et al. The IL-33-PIN1-IRAK-M axis is critical for type 2 immunity in IL-33-induced allergic airway inflammation. *Nat Commun*. 2018;9(1):1603. doi:10.1038/s41467-018-03886-6
44. Izuishi K, Tsung A, Jeyabalan G, et al. Cutting edge: high-mobility group box 1 preconditioning protects against liver ischemia-reperfusion injury. *J Immunol*. 2006;176(12):7154–7158. doi:10.4049/jimmunol.176.12.7154
45. Li C, Jiang M, Fang ZT, et al. Current evidence of synaptic dysfunction after stroke: cellular and molecular mechanisms. *CNS Neurosci Ther*. 2024;30(5):e14744. doi:10.1111/cns.14744
46. Zhou Y, Wang Y, Wang J, Anne Stetler R, Yang QW, Inflammation in intracerebral hemorrhage: from mechanisms to clinical translation. *Prog Neurobiol* 2014;115:25–44. doi:10.1016/j.pneurobio.2013.11.003
47. Cao C, Ding J, Cao D, et al. TREM2 modulates neuroinflammation with elevated IRAK3 expression and plays a neuroprotective role after experimental SAH in rats. *Neurobiol Dis*. 2022;171:105809. doi:10.1016/j.nbd.2022.105809
48. Li X, Chen G, CNS-peripheral immune interactions in hemorrhagic stroke. *J Cereb Blood Flow Metab*. 2023;43(2):185–197. doi:10.1177/0271678X221145089
49. Li X, Bechara R, Zhao J, McGeachy MJ, Gaffen SL, IL-17 receptor–based signaling and implications for disease. *Nat Immunol*. 2019;20(12):1594–1602. doi:10.1038/s41590-019-0514-y
50. Waisman A, Hauptmann J, Regen T, The role of IL-17 in CNS diseases. *Acta Neuropathol*. 2015;129(5):625–637. doi:10.1007/s00401-015-1402-7
51. Lv M, Liu Y, Zhang J, et al. Roles of inflammation response in microglia cell through Toll-like receptors 2/interleukin-23/interleukin-17 pathway in cerebral ischemia/reperfusion injury. *Neuroscience*. 2011;176:162–172. doi:10.1016/j.neuroscience.2010.11.066
52. Fei X, Wang L, Dou YN, et al. Extracellular vesicle encapsulated homer1a as novel nanotherapeutics against intracerebral hemorrhage in a mouse model. *J Neuroinflammation*. 2024;21(1):85. doi:10.1186/s12974-024-03088-6
53. Nakamura T, Hua Y, Keep RF, Park JW, Xi G, Hoff JT, Estrogen therapy for experimental intracerebral hemorrhage in rats. *J Neurosurg*. 2005;103(1):97–103. doi:10.3171/jns.2005.103.1.0097